Economic Geology, v. 112, pp. 829–853

Re-Os and U-Pb Geochronology of the Doña Amanda and Cerro Kiosko Deposits, Bayaguana District, Dominican Republic: Looking Down for the Porphyry Cu-Mo Roots of the Pueblo Viejo-Type Mineralization in the Island-Arc Tholeiitic Series of the Caribbean*

Lisard Torró,[1,†] Antoni Camprubí,[2] Joaquín A. Proenza,[1] Paulo León,[3] Holly J. Stein,[4,5] John F. Lewis,[6] Carl E. Nelson,[7] Cevero Chavez,[3] and Joan Carles Melgarejo[1]

[1] *Departament de Mineralogia, Petrologia i Geologia Aplicada, Facultat de Geologia, Universitat de Barcelona (UB), Martí i Franquès s/n, 08028 Barcelona, Spain*

[2] *Instituto de Geología, Universidad Nacional Autónoma de México, Ciudad Universitaria, 04510 Ciudad de México, Mexico*

[3] *Corporación Minera Dominicana, C/ José A. Brea Peña #14, Edificio District Tower, Level 3, Ensanche Evaristo Morales, Santo Domingo, Dominican Republic*

[4] *AIRIE Program, Department of Geosciences, Colorado State University, Fort Collins, Colorado 80523*

[5] *Centre for Earth Evolution and Dynamics (CEED), University of Oslo, Norway*

[6] *Department of Earth and Environmental Sciences, George Washington University, Washington, D.C., 20052*

[7] *Recursos del Caribe, S.A., 2360 23rd Street, Boulder, Colorado 80304*

Abstract

Hosted in the Early Cretaceous bimodal tholeiite volcanic series of the Los Ranchos Formation, the Doña Amanda and Cerro Kiosko deposits in the Bayaguana district represent significant Au, Cu, and Ag resources in the Cordillera Oriental of the Dominican Republic. At Doña Amanda, a dense stockwork of quartz-sulfide veins is hosted by volcanic rocks with intense transitional phyllic-advanced argillic and silicic hydrothermal alteration assemblages, indicating a high-sulfidation environment. Wavy quartz veins with central sutures and rims of pyrite + enargite + molybdenite + fahlore (B veins) are cut by planar quartz-pyrite D veins. Primary fluid inclusions in quartz from B veins (Th: 160°–>400°C; salinity: 7.9–16.4 wt % NaCl equiv) are interpreted as porphyry-type fluids. Inclusion fluids in quartz of quartz-pyrite veins (Th: 125°–175°C; salinity: 4.8–12.2 wt % NaCl equiv), quartz from silicic altered wall rocks (Th: 150°–175°C; salinity: 8.3–13.9 wt % NaCl equiv), and late, distal calcite veins (Th: 120°–160°C; salinity: 5.0–13.3 wt % NaCl equiv) indicate limited mixing with more dilute fluids and rule out mixing with fresh meteoric water. In Cerro Kiosko, a swarm of fault-controlled massive chalcopyrite + enargite + bornite + fahlore D veins and lodes are hosted by rocks with pervasive kaolinite alteration after sericite. $\delta^{34}S$ values of vein sulfides from both deposits are all close to –2‰ and consistent with a predominance of magmatic sulfur and sulfide deposition from an oxidizing magmatic fluid. These data are consistent with a transitional environment between a deeper porphyry Cu(-Mo) and an overlying high-sulfidation epithermal deposit.

An Re-Os age (112.6 ± 0.4 Ma) for molybdenite from the Doña Amanda deposit places the porphyry-epithermal mineralization as Early Cretaceous, coeval with the Los Ranchos Formation host rocks and with the Pueblo Viejo deposit. New sensitive high-resolution ion microprobe U-Pb ages on zircons from plagioclase-phyric rhyolite domes in the Bayaguana district are consistent with porphyry–high-sulfidation epithermal mineralization occurring along the Los Ranchos Formation during tonalite batholith emplacement in the basaltic island-arc basement at ca. 118 to 112 Ma and finalization of felsic volcanism at ca. 110 to 107 Ma.

Introduction

Extensive exploration since the early 1970s for precious and base metals in Cretaceous volcanic and volcanosedimentary series along the Cordillera Central-Massif du Nord (as defined by Lewis and Draper, 1990) and the Cordillera Oriental of Hispaniola Island (Dominican Republic and Haiti) has revealed the existence of major mineral resources (Kesler et al., 1990; Nelson et al., 2011). The Cordillera Central contains the world-class Pueblo Viejo Au-Ag-Cu deposit, with 8,960,000 oz Au of proven and probable reserves and a reported production of 572,000 oz Au in 2015 (Barrick, 2015), and also the Cerro de Maimón Au-Ag-Cu (Lewis et al., 2000; Torró et al., 2016) and Falcondo Ni (Nelson et al., 2011; Aiglsperger et al., 2016) deposits. With the resumption of operations at Pueblo Viejo in 2012 by Barrick-Goldcorp Inc., the Dominican Republic is becoming a major gold producer (Redwood, 2014, 2015). Continued mining exploration, mainly for gold, is leading to new discoveries such as the Romero and Romero South deposits, with indicated resources of 2.4 Moz Au equiv (GoldQuest, 2015; Román-Alday et al., 2015), and a 2-Moz Au inferred resource at Candelones (Unigold, 2015).

The Bayaguana district, about 65 km northeast of Santo Domingo (Fig. 1), contains the most promising, albeit poorly understood, metallic mineralization in the Cordillera Oriental of the Dominican Republic. Perilya-CORMIDOM has developed extensive exploration programs that followed previous

† Corresponding author: e-mail, lisardtorro@hotmail.com

* A digital supplement to this paper is available at http://economicgeology.org/ and at http://econgeol.geoscienceworld.org/.

Submitted: July 29, 2016
Accepted: October 31, 2016

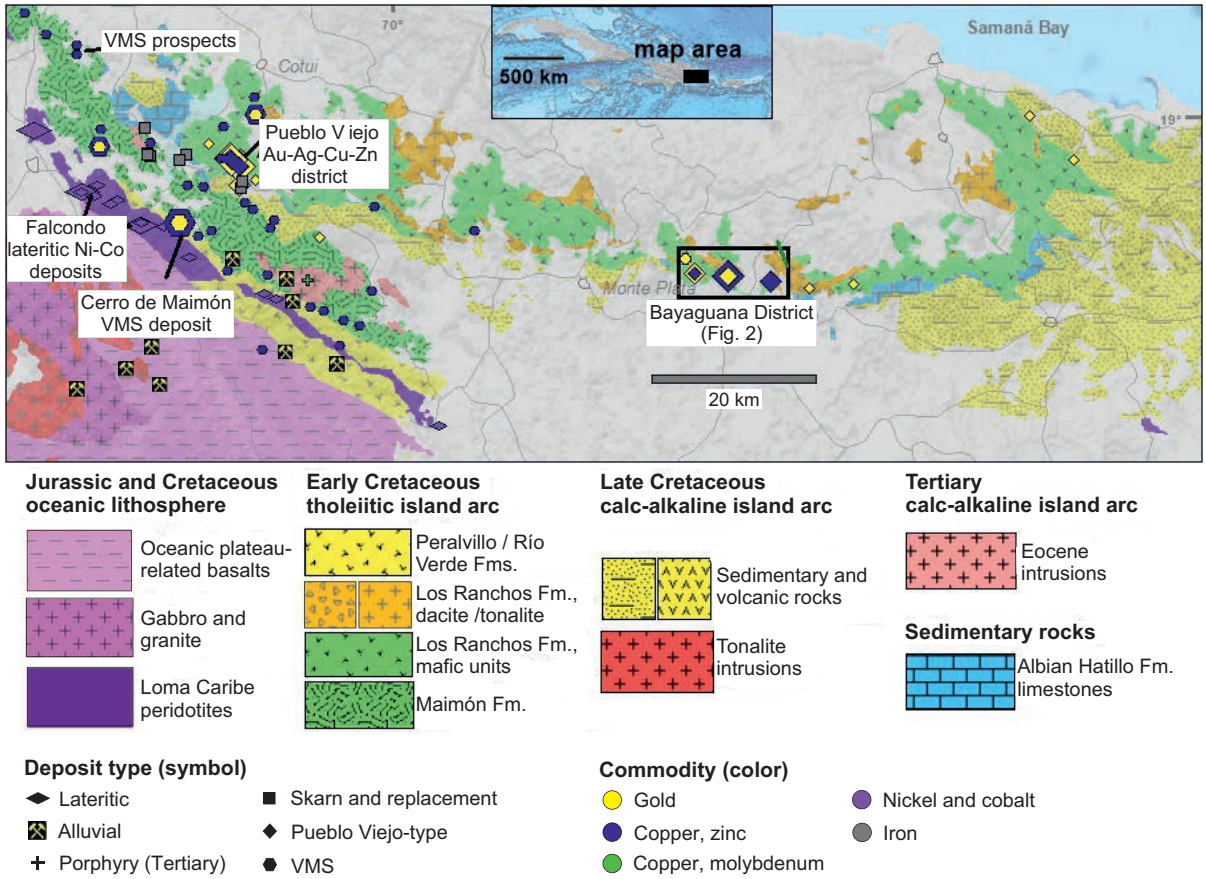

Fig. 1. Location map for the Los Ranchos Formation and the Bayaguana district in the Dominican Republic. The geologic base map was modified from Toloczyki and Ramirez (1991).

efforts commenced by the Dominican Mining Department (Dirección General de Minería) and Falconbridge Ltd. in the 1980s and 1990s. Inferred resources include Cerro Kiosko (2.8 Mt at 2.2 g/t Au, 4.7 g/t Ag, 0.6% Cu) and Doña Amanda (54.62 Mt at 0.37% Cu, 0.23 g/t Au, 1.42 g/t Ag); other noted occurrences are at Doña Loretta (24.14 m at 2.03% Cu, 0.39 g/t Au, 4.55 g/t Ag; 15.25 m at 1.09% Cu, 0.20 g/t Au, 1.82 g/t Ag) and intercepts in the Loma Guaymarote basin (e.g., 6.35 m at 1.37 g/t Au; Chénard, 2006; Perilya, 2015). The rocks hosting these ores in Perilya's concessions in Bayaguana are part of the Early Cretaceous Los Ranchos Formation, renowned for hosting the Pueblo Viejo (Moore, Monte Negro, and Monte Oculto deposits) district (Fig. 1).

Although it is widely accepted that Pueblo Viejo mineralization was coeval with bimodal tholeiitic volcanism and epiclastic sedimentation of the Los Ranchos Formation (Kesler et al., 2005a, b; Mueller et al., 2008; Kirk et al., 2014; Nelson et al., 2015), an Early Cretaceous age has not been universally acknowledged (e.g., Sillitoe et al., 2006, 2007). Controversies over the origin of the Pueblo Viejo deposit (cf. Nelson et al., 2011, 2015) have caused notable confusion for geologists engaged in exploration of the Los Ranchos Formation. Kesler et al. (2005b) and Kirk et al. (2014) noted that the association between the Pueblo Viejo deposit and primitive tholeiitic magmatism in the Caribbean island arc makes it questionable as to whether these magmas were capable of forming multiple epithermal deposits, or whether Pueblo Viejo should be regarded as an isolated anomaly, making further exploration unlikely to be successful. With that in mind, we evaluate the formation of the ore deposits hosted by the Los Ranchos Formation by assessing their relationships to regional-scale features. New whole-rock geochemical data are provided for the ore-hosting volcanic rocks. Mineralization at Doña Amanda and felsic domes in the Bayaguana district have been dated by means of Re-Os (molybdenite) and U-Pb (zircon) techniques, respectively. The mineralogy (ore, gangue, and alteration), sulfur isotopes, and the thermochemical characteristics of mineralizing fluids in the deposits of the Bayaguana district are assessed to help develop a genetic model. These results are combined to provide local and regional exploration guidelines and insights into the Caribbean island arc evolution.

Geologic Setting

Located on the northern margin of the Caribbean plate, Hispaniola Island is a tectonic collage of mantle and crustal units resulting from the WSW- to SW-directed oblique convergence of the continental margin of the North American plate with the Circum-Caribbean island arc since the Eocene (Lewis and Draper, 1990; Boschman et al., 2014; Lidiak and Anderson, 2015). The Bayaguana concessions (named, from west to east, La Hiena, Bayajá, and Los Mameyes) cover approximately 7,200 hectares of the Early Cretaceous Los

Ranchos Formation in its eastern extension in the Cordillera Oriental, about 70 km to the east-southeast of the Pueblo Viejo deposit (Fig. 1). The Los Ranchos Formation, together with the Maimón and Amina formations, records the oldest and chemically most primitive island-arc volcanism in the Caribbean region (Lewis and Draper, 1990; Kesler et al., 1991; Lewis et al., 2002; Escuder-Viruete et al., 2006, 2007). They constitute the basement in central Hispaniola. Boninitic and tholeiitic magmatism in these formations and other equivalent units in the Greater Antilles are commonly grouped as the primitive island-arc magmatic suite, deposited at ca. 135 to 110 Ma. Boninitic and tholeiitic magmatism, in general, predates the more voluminous calc-alkaline magmatic suite formed between ca. 95 and 45 Ma (Lidiak and Anderson, 2015, and references therein). Subduction of the North American plate beneath the Greater Antilles island-arc and related arc magmatism ceased in Hispaniola in the Eocene with the collision of the arc and the Bahamas Platform (Mann et al., 1991; Boschman et al., 2014). In the eastern Cordillera Central, transpressional WNW-ESE faults accommodated arc-continent collision in Hispaniola and juxtaposed the arc-related Los Ranchos, Maimón, Peralvillo, and Río Verde formations with Caribbean-derived mantle peridotites of Loma Caribe (Marchesi et al., 2016, and references therein) and Caribbean-Colombian oceanic plateau enriched mid-ocean ridge basalts (E-MORB) represented by the Duarte, Siete Cabezas, and Pelona-Pico Duarte formations (Fig. 1; Escuder-Viruete et al., 2008).

Los Ranchos Formation

The Los Ranchos Formation crops out as an arched, 100-km-long belt that extends from the Hatillo reservoir (Cotuí-Pueblo Viejo area) eastward to the south shore of Samaná Bay (Fig. 1; Kesler et al., 1991). It is composed of a volcanic pile of Early Cretaceous bimodal volcanic, volcaniclastic, and minor sedimentary rocks with a stratigraphic thickness of >3 km at Pueblo Viejo (Bowin, 1966; Kesler et al., 1991; Escuder-Viruete et al., 2006, 2007). The volcanic sequence was intruded by tonalite batholiths and diorite to gabbro plutons and dikes of apparent Paleocene age, particularly in the Cordillera Oriental area, as mapped by the European SYSMIN Project-L (Escuder-Viruete et al., 2006). In the Cevicos-Miches area, Escuder-Viruete et al. (2006, 2007) subdivided the Los Ranchos Formation into (1) a lower basaltic unit dominated by spilitized volcanic breccias and flows with local pillow lavas and interbedded fine volcaniclastic rocks, (2) an intermediate rhyodacitic unit composed of dacite to rhyolite flows, brecciated volcanic domes, and minor felsic tuffs, and (3) an upper basaltic unit composed of massive flows of basalt to andesite, autoclastic breccias, and synvolcanic gabbros locally overlain by dacitic to rhyolitic flows and domes and associated autoclastic breccias (Fig. 2B). The Los Ranchos Formation in the Pueblo Viejo area was described by Kesler et al. (1991) as (1) the basal Cotuí Member, characterized by spilitic pillow lavas and lava flows, (2) the Quita Sueño Member, consisting largely of keratophyric acid flows and minor tuffs and shallow intrusions, (3) the Meladito fragmental member, with a complex stratigraphy including very coarse grained debris flows that grade upward to lithic and bedded tuffs, and (4) the Platanal spilite member, composed of spilitized mafic flows (without pillows) and minor volcaniclastic breccias. The Meladito and Platanal members are cut by (5) the Zambrana fragmental member, interpreted to have formed in a phreatomagmatic eruption in an emergent volcano (Kesler et al., 1991), and (6) the Pueblo Viejo Member, which hosts the bulk of the ores at Pueblo Viejo and is composed of volcanogenic and terrestrial sediments with Early Cretaceous plant fossils (Russell and Kesler, 1991; Smiley, 2002). The Pueblo Viejo sedimentary rocks were intruded by (7) andesite to dacite porphyritic domes and dikes (Nelson, 2000; Mueller et al., 2008).

Escuder-Viruete et al. (2006, 2007) described basalts of the basal unit as boninites and light rare earth element (LREE)-depleted island-arc tholeiites, with normalized rare earth element (REE) patterns and TiO_2 contents markedly different from those of basalts from the upper unit, identified as normal island-arc tholeiites. Low-K and near-flat normalized REE patterns of acid rocks from the intermediate unit determined their tholeiitic affinity and the possibility that they formed as a product of secondary melting at the base of the early arc crust. Escuder-Viruete et al. (2006) concluded that the Los Ranchos Formation records the subduction zone initiation in the Caribbean island arc, and that the upper basalts formed after the subsequent establishment of the volcanic front, simultaneously with the shallowing of the arc volcanic and volcanosedimentary edifice.

The age of the Los Ranchos Formation was first constrained to ca. 130 to 110 Ma through Pb isotope ratios on 17 rock samples by Cumming et al. (1982) and Cumming and Kesler (1987). This range was largely coincident with the Early Cretaceous ages proposed by Smiley (2002) from the study of terrestrial fossil plants, and the middle Aptian to middle Albian age by Bowin (1966) for marine fossils, both in the upper levels of the Los Ranchos Formation. Bellon et al. (1985) obtained a K-Ar age of 112.4 ± 11 Ma for a basalt sample of the Los Ranchos Formation at El Seibo, in the Eastern Peninsula (formerly identified as the El Seibo unit). Kesler et al. (2005a) reported U-Pb ages of 113.9 ± 0.8 or 118.6 ± 0.5 Ma (depending on interpretation of the data) for a quartz-feldspar porphyry from the Quita Sueño Member, and an age of 110.9 ± 0.8 Ma for a quartz-porphyry fragmental rock in the Pueblo Viejo Member. The Cotuí stock intruded at 111.8 ± 0.6 or 112.9 ± 0.9 Ma (Kesler et al., 2005a). Quartz porphyries in the upper Los Ranchos Formation yielded a U-Pb zircon age of 111.4 ± 0.5 Ma (Kesler et al., 2005b), which is largely coincident with the age of intrusion of the Cotuí stock. Escuder-Viruete et al. (2006, 2007) obtained a U-Pb zircon age of 116.0 ± 0.8 Ma from a porphyritic rhyodacite from the intermediate rhyodacitic unit in Bayaguana, close to the Doña Loretta prospect, and 115.5 ± 0.3 Ma for a tonalite from the Zambrana batholith, which intruded the Los Ranchos Formation in the Cotuí-Maimón area. In addition, these authors reported $^{40}Ar/^{39}Ar$ plateau ages for hornblende in tonalites mostly in the 109 to 106 Ma range and interpreted them as final cooling ages. Mueller et al. (2008) obtained a U-Pb age at 109.6 ± 0.6 Ma for the youngest zircon population from an intermineralization andesite porphyry dike in the Pueblo Viejo deposit. The age of the Los Ranchos Formation is further constrained by the overlying Hatillo Formation, composed of clastic deposits at its base, which grade upward to a massive micritic reef sequence that was deposited

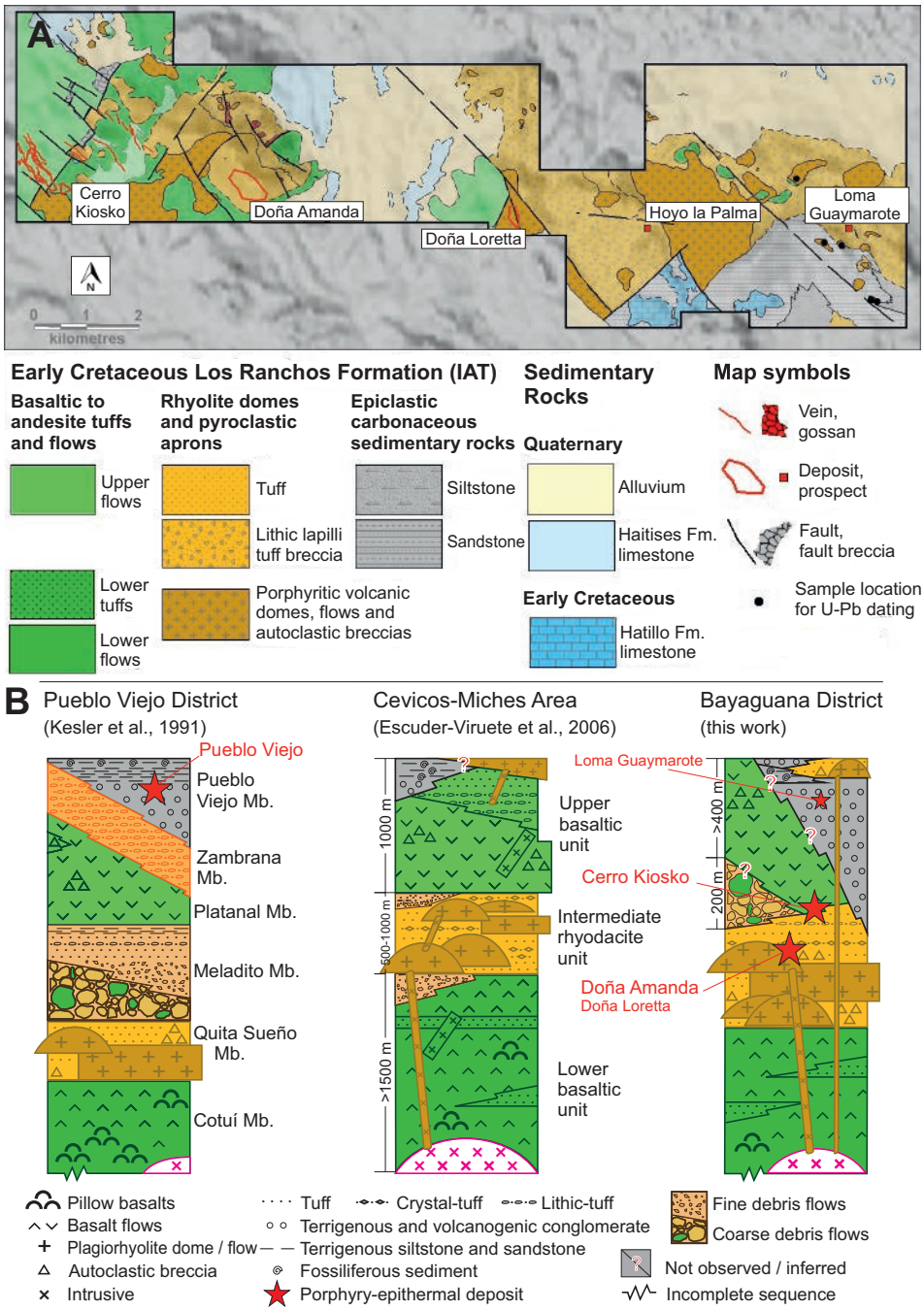

Fig. 2. (A) Geologic map of the Bayaguana district (see Fig. 1 for location) showing the Doña Amanda and Cerro Kiosko deposits and the Doña Loretta, Hoyo La Palma, and Loma Guaymarote mineralization and prospects. Red contours represent the vertical projection of the deposit limits on surface. Sample locations for U-Pb dating (zircon) in plagioclase-phyric rhyolite domes from the Loma Guaymarote area are also shown. (B) Schematic lithostratigraphic columns for the Los Ranchos Formation in the Pueblo Viejo district (Kesler et al., 1991), the Cevicos-Miches area (Escuder-Viruete et al., 2006), and the Bayaguana district (this study). IAT = island-arc tholeiite.

in shallow-water conditions during Albian time (Russell and Kesler, 1991; Kesler et al., 2005a, b; Myczynski and Iturralde-Vinent, 2005). Invertebrate fauna at the base of the Hatillo Formation was dated as late lower Albian by Myczynski and Iturralde-Vinent (2005). The deposition of the Hatillo Formation could be partly coeval with the last stages of magmatism of the Los Ranchos Formation and with ore deposition at Pueblo Viejo, based on the occurrence of hydrothermal alteration at the base of the Hatillo Formation identified by Sillitoe et al. (2006; cf. Kirk et al., 2014; Nelson et al., 2015).

Geology of the Bayaguana district

Detailed mapping of the Bayaguana district and a drilling campaign of target areas indicate conspicuous heterogeneity

of volcanic and sedimentary rock units. Massive flows of plagioclase- and moderately pyroxene-phyric, sparsely amygdaloidal, locally pillowed basalts and minor hyaloclastites are grouped into the lower basaltic unit. This unit crops out extensively in the western portion of the study area (Fig. 2A). Drill core intersections indicate that it extends for >15 km farther east, to the Loma Guaymarote prospect, and underlies the felsic and the upper basaltic andesite and andesite units. Interstratified basaltic fine tuffs in the lower basaltic unit are consolidated, thinly bedded horizons that are up to 50 m thick. The upper basaltic and andesitic unit is composed of massive dark green plagioclase- and pyroxene-phyric basaltic andesite and andesite flows with minor lateral autobreccias and local massive to stratified crystal-rich volcanic breccias. This unit crops out widely in the westernmost sector of the concessions, in fault contact with the lower basaltic unit, but is more restricted in the central part of the district (Fig. 2A). As observed in drill cores, the upper basaltic and andesitic unit is >400 m thick.

Large volumes of felsic-intermediate volcanic deposits are the most abundant host rocks in the Bayaguana district. They have been mapped as massive lava flows, domes, reworked pyroclastic aprons, breccias, and tuffs that intruded and covered the lower basaltic unit basement. Plagioclase-phyric rhyolite flows and domes crop out in the western and, more abundantly, in the eastern sectors of the district. Rhyolite lava flows and coherent cores of domes contain abundant coarse-grained quartz-, medium-grained plagioclase-, and fine-grained pyroxene-phyric textures in a microcrystalline quartz groundmass. These rocks have been affected by intense silicic, phyllic, and argillic alteration. Massive plagioclase-phyric rhyolite flows and domes are visible as smooth hillocks. The domes are spatially restricted and commonly exhibit lateral carapaces or aprons of partially reworked autobreccias and lithic or crystal tuffs (Fig. 2). Compacted felsic lithic and crystal tuffs with moderate argillic alteration are distributed widely in the western sector of the district, where they overlie the rhyolite flows. The volcanic series is overlain by up to 200 m of volcanogenic sedimentary deposits with dm-sized basalt, plagioclase-phyric rhyolite, and felsic tuff fragments in a coarse crystal- and lithic-rich matrix. This unit is commonly intersected by drilling in the central and eastern areas of the district.

In the Loma Guaymarote area, there is a ~3-km-long and 2.4-km-wide Early Cretaceous sedimentary basin (i.e., about four times the size of an equivalent basin in the Pueblo Viejo district), which is up to 241 m thick (Fig. 2). Volcanogenic and terrigenous sedimentary rocks of the upper Los Ranchos Formation (i.e., the Pueblo Viejo Member) record lateral changes of facies from lithic conglomerates with felsic volcanic rock fragments to quartz sandstones to sandy siltstones and local carbonaceous mudstones. Sedimentary rocks generally overlie or are in fault contact with plagioclase-phyric rhyolite massive flows and volcanogenic breccias. They have been intruded by plagioclase-phyric rhyolite domes and are locally interstratified with dome autobreccias and lithic-tuff aprons. Micritic, reefal Hatillo limestones, an important marker bed along the Los Ranchos belt (Mczynski and Iturralde-Vinent, 2005), overlie the rocks of the sedimentary basin.

The Doña Amanda deposit (Fig. 2) consists of a ~100-m-thick supergene enrichment blanket (chalcocite and covellite) that overlies strongly silicified and mineralized felsic pyroclastic rocks intruded by plagioclase-phyric rhyolite at depth. Its hypogene mineralization is composed of a dense stockwork of quartz-sulfide Cu-Mo veins and includes sulfide disseminations. The Cerro Kiosko deposit (Fig. 2) consists of a 1.25- to 22-m-thick, ~1,100-m-long, and ~400-m-deep tabular quartz-sulfide vein swarm hosted by silicic-altered basaltic andesites and andesites of the upper unit, and also includes sulfide disseminations. The vein swarm is composed of stringers and massive sulfide lodes largely controlled by NW-striking normal faults that dip ~60° to the southwest (Chénard, 2006). Other areas of mineralization in the Bayaguana district include the Doña Loretta prospect, which contains broad zones of silicic and argillic alteration of the volcanic rocks, and the Loma Guaymarote prospect, a sulfide-bearing stockwork that overprints argillic-altered sedimentary rocks of the upper Los Ranchos Formation.

Volcanic Lithogeochemistry

Igneous rocks from the Maimón and Los Ranchos formations are considered to be representative of the most primitive island-arc tholeiite magmatic series in the Caribbean region (Lidiak and Anderson, 2015). Lithogeochemical datasets including major and trace element compositions of volcanic rocks from the Maimón Formation were generated by Lewis et al. (2000, 2002) and Torró et al. (2017, in press), whereas only Escuder-Viruete et al. (2006) have previously generated data for the Los Ranchos Formation. The genetic correlation between these two formations is still a matter of debate. Escuder-Viruete et al. (2007), for example, advocated for the formation of both units in an equivalent position in the arc-forearc portion because of their similar geochemical signatures. On the other hand, the occurrence of porphyry-epithermal mineralization in the Los Ranchos Formation, in stark contrast to volcanogenic massive sulfide (VMS) mineralization hosted in the Maimón Formation, led other authors to envisage different positions of formation for both units (e.g., Nelson et al., 2011; Torró et al., 2016). In order to better assess similarities and differences between the lithogeochemistry of rocks from both formations and to judge the geochemical affinity of the mineralization hosts, we report new, unpublished data on volcanic rocks from the Los Ranchos Formation in the Bayaguana area. This study is based on 51 rock samples. Selected rock samples are representative of massive flows from the lower basaltic unit, rhyolites from the intermediate unit, and basaltic andesites and andesites from the upper unit. Major, minor, and trace elements were determined by X-ray fluorescence (XRF) and inductively coupled plasma-mass spectrometry (ICP-MS; 4A and 4B packages; lithium borate fusion) at ACME Labs, Vancouver, Canada, and at the Centro de Instrumentación Científica of the University of Granada, Spain (see Torró et al., 2016, for technical details). Representative analyses of the different lithotypes are presented in Table 1 and are described below.

Rocks of the Los Ranchos Formation have undergone extensive seafloor metamorphism (forming spilites and keratophyres; e.g., Kesler et al., 1991; Lewis et al., 2002; Escuder-Viruete et al., 2006). In addition, in the Bayaguana and Pueblo Viejo districts, most rocks have intense hydrothermal alteration associated with the formation of the ore deposits (e.g., Kesler

Table 1. Representative Whole-Rock Geochemical Data for the Different

Lab.[1]	ACME	ACME	CIC-UGR	CIC-UGR	ACME	CIC-UGR	CIC-UGR	ACME	CIC-UGR	ACME	ACME	ACME
Original rock type	Basalt	Basalt	Basalt	Basalt	Basalt	Basalt	Basaltic andesite	Basaltic andesite	Basaltic andesite	Basaltic andesite	Andesite	Andesite
Affinity	LOTI	LOTI	LOTI	LOTI	LOTI	IAT						
DDH[2] (depth)	Outcrop	CC-18 (73.0)	DA-23 (18.6)	OF-47 (282.5)	OF-04 (151.1)	OF-01 (229.5)	HP-01 (120.0)	LG-02 (123.0)	LG-02 (45.8)	LG-04 (133.0)	CC-27 (74.8)	DA-15 (97.0)
Elevation[3] (m)		155	270	82	97	124	230	169	169	174	160	220
Azimuth/dip[3]		40 / -50	0 / -55	60 / -55	60 / -50	60 / -50	230 / -60	40 / -50	40 / -50	40 / -50	40 / -50	60 / -70
UTM E[3]	433991	439396	434561	430497	430135	430308	442223	444243	444243	443839	439572	433980
UTM N[3]	2080155	2082576	2080032	2080587	2081068	2081168	2079836	2079360	2079360	2078538	2080120	2081279
Sample no.	B2013-005	CC-18-73	DA-23-1	OF-47-282,50	OF-04-151.1	OF-01-229,55	HP-01-7	LG-02-123	LG-02-2	LG-04-133	CC-27-74.80	DA-15-97
SiO_2	52.72	54.32	50.50	48.16	48.92	51.36	59.26	61.05	63.82	58.00	71.51	56.25
Al_2O_3	17.31	15.89	19.99	16.18	17.77	18.84	14.72	15.57	14.60	15.01	14.42	16.51
Fe_2O_3	5.79	9.72	7.94	10.88	10.14	10.25	7.05	6.31	6.05	6.81	3.19	8.37
MnO	0.12	0.11	0.12	0.20	0.17	0.19	0.10	0.12	0.12	0.08	0.09	0.25
MgO	1.61	7.19	4.79	7.83	4.70	3.01	3.49	5.15	3.19	3.84	1.90	3.55
CaO	16.18	1.58	10.37	11.11	8.79	6.68	6.68	1.59	3.07	7.35	0.12	8.80
Na_2O	0.06	3.52	2.48	1.75	3.79	3.53	2.46	1.98	4.65	3.21	4.55	1.40
K_2O	0.01	0.28	0.29	0.05	0.35	1.19	1.02	2.75	0.37	0.18	0.46	0.08
TiO_2	0.74	0.51	0.63	0.61	0.62	0.91	0.60	0.54	0.56	0.52	0.37	0.68
P_2O_5	0.09	0.05	0.06	0.06	0.05	0.16	0.07	0.08	0.07	0.08	0.03	0.06
LOI	5.30	6.60	2.32	2.44	4.50	3.05	4.09	4.70	2.63	4.80	3.10	3.80
Total	99.93	99.77	99.49	99.27	99.80	99.17	99.54	99.84	99.13	99.88	99.74	99.75
Rb	0.05	1.8	3.2	1.2	5.4	14.6	7.9	26.8	5.0	1.9	5.0	0.70
Cs	0.05	0.20	0.51	0.42	0.40	1.3	0.52	1.3	0.15	0.20	0.10	0.05
Sr	20	90	217	374	353	370	111	52	39	147	75	346
Ba	23	49	100	47	164	340	207	315	54	82	84	32
Sc	39	36	49	48	39	33	31	28	30	28	22	31
V	355	255	339	287	310	217	198	169	128	182	23	256
Cr	6.8	34.2	46.3	156.3	41.1	3.5	35.7	20.5	21.6	20.5	6.8	13.7
Co	10.2	39.1	25.1	39.8	28.5	22.0	20.8	15.1	16.7	16.0	2.7	19.5
Ni	3.6	21.6	24.8	60.8	<20	10.5	20.2	6.9	9.7	7.9	1.4	5.5
Cu	22	26	83	78	81	77	61	43	28	8	2068	73
Zn	56	59	80	70	64	93	83	57	58	52	172	281
Ga	16.8	13.3	15.7	14.2	17.2	18.4	13.6	12.5	12.7	13.1	11.9	15.3
Y	16.2	15.3	11.4	11.3	13.9	23.1	23.2	19.5	23.4	22.7	33.8	18.1
Nb	0.50	0.20	0.31	0.25	0.40	0.72	0.48	0.50	0.52	0.30	0.90	0.70
Ta	0.05	0.05	0.08	0.06	0.10	0.07	0.07	0.05	0.09	0.05	0.05	0.05
Zr	33	21	10	11	24	33	56	59	66	59	71	56
Hf	1.3	0.60	0.60	0.65	0.70	1.3	2.0	2.2	2.2	2.3	2.8	1.7
Mo	0.60	0.05	0.28	0.33	0.20	0.39	0.35	0.30	0.10	0.20	0.40	1.1
Sn	0.50	1.0	0.36	0.38	1.0	0.59	0.58	0.50	1.1	0.50	0.50	0.50
Tl	0.05	0.05	0.03	0.02	0.10	0.13	0.06	0.05	0.04	0.05	0.05	0.05
Pb	0.50	1.1	0.56	0.98	1.1	1.64	1.78	0.70	0.98	1.1	0.50	2.5
U	0.05	0.05	0.03	0.07	0.10	0.17	0.18	0.20	0.26	0.50	0.60	0.20
Th	0.10	0.10	0.07	0.19	0.30	0.40	0.32	0.30	0.38	0.20	0.30	0.40
La	2.4	1.0	0.92	1.4	2.9	3.4	2.0	2.5	1.9	2.0	4.3	4.6
Ce	5.3	2.0	2.4	3.4	5.8	8.2	5.5	5.2	5.6	5.2	11.4	9.8
Pr	0.93	0.48	0.43	0.57	0.91	1.3	0.96	0.98	0.94	0.99	1.9	1.6
Nd	5.9	3.1	2.6	3.2	4.3	7.5	5.7	5.3	5.4	5.8	10.2	8.7
Sm	1.6	1.3	1.1	1.1	1.4	2.5	2.2	1.9	2.1	1.9	3.0	2.3
Eu	0.69	0.46	0.46	0.48	0.63	1.1	0.65	0.56	0.57	0.64	0.93	0.80
Gd	2.7	2.1	1.4	1.4	1.8	3.1	2.7	2.7	2.6	2.9	4.3	3.0
Tb	0.44	0.40	0.25	0.27	0.35	0.55	0.49	0.49	0.48	0.54	0.80	0.51
Dy	3.1	2.9	1.8	1.8	2.4	3.8	3.6	3.6	3.7	4.0	5.5	3.4
Ho	0.65	0.67	0.40	0.42	0.46	0.85	0.83	0.77	0.87	0.86	1.2	0.70
Er	2.1	1.8	1.1	1.1	1.5	2.3	2.5	2.3	2.5	2.5	3.6	2.1
Tm	0.28	0.27	0.18	0.19	0.23	0.41	0.39	0.32	0.43	0.41	0.55	0.29
Yb	1.5	1.7	1.2	1.2	1.4	2.5	2.6	2.5	2.7	2.8	3.4	2.0
Lu	0.26	0.28	0.19	0.19	0.20	0.39	0.41	0.39	0.43	0.44	0.61	0.29
AI[4]	9.0	59.4	28.3	38.0	28.6	29.1	33.0	68.9	31.6	27.6	33.6	26.2
CCPI[5]	99.1	80.7	81.2	90.7	77.0	72.2	73.9	69.6	63.2	74.6	48.8	88.2
AAAI[6]	22.8	30.7	22.3	18.9	22.1	28.0	31.9	41.2	36.9	28.7	52.1	29.0

Concentrations of oxides are given in wt %; other data are in ppm; IAT = island-arc tholeiite; LOTI = low-Ti tholeiite

[1] Lab. refers to the two labs where the chemical analyses were done; ACME Labs = ACME Laboratories, Vancouver, Canada; CICUGR = Centro de Instrumentacion Cientifica of the University of Granada

[2] DDH refers to the diamond drill holes from which the samples were collected; surface samples are identified as "outcrop"

[3] For DDH samples, elevation (m.a.s.l.) and coordinates refer to the location of collars, and azimuth and elevation refer to the drill core orientation and inclination; UTM zone 19 (NAD27 for US); all analyzed samples are in the Bayaguana (6272-II) 1:50,000 sheet

Lithological Groups of Volcanic Rocks Studied from the Bayagyana District

ACME	ACME	ACME	ACME	ACME	ACME	ACME	ACME	ACME	ACME	ACME	CIC-UGR	ACME
Andesite	Andesite	Andesite	Andesite	Andesite	Andesite	Rhyolite	Rhyolite	Rhyolite	Rhyolite	Rhyolite	Rhyolite	Rhyolite
DA-17 (122.0) 185 0 / -60 433980 2081279 DA-17-122	Outcrop 433931 2082222 RMN-13-025	Outcrop 433612 2083942 RMN-13-049	OF-32 (170.0) 115 60 / -55 431825 204481 OF-32-170	OF-26 (50.0) 125 60 / -55 432045 2082173 OF-26-50	Outcrop Bay14-014	Outcrop 430852 2080448 B2013-001	Outcrop 431527 2080277 B2013-003	CC-18 (53.9) 155 40 / -50 439396 2082576 CC-18-53.85	CC-29 (244.5) 185 40 / -60 439550 2080465 CC-29-244.5	HP-01 (296.5) 230 230 / -60 442223 2079836 HP-01-296.5	HP-01 (28.0) 230 230 / -60 442223 2079836 HP-01-1	LG-22 (76.5) 139 40 / -45 446812 2079387 LG-22-76.5
58.81	76.44	61.07	64.45	56.06	58.14	75.80	79.05	74.02	70.59	73.63	77.48	75.04
16.20	16.90	16.04	15.26	16.14	17.35	11.95	10.76	12.46	11.75	12.74	10.44	11.74
6.96	0.20	6.45	5.14	10.28	8.12	2.61	2.17	3.20	3.78	3.46	2.72	2.36
0.21	0.01	0.15	0.12	0.30	0.13	0.05	0.03	0.03	0.07	0.08	0.08	0.06
3.22	0.01	3.14	2.26	3.61	2.38	0.51	0.40	1.11	1.49	2.29	1.90	0.37
5.14	0.07	4.94	2.76	1.74	1.97	0.47	0.29	1.03	3.35	0.45	0.63	2.68
3.80	0.04	4.53	3.70	3.32	6.17	3.67	3.87	5.68	2.90	3.19	3.28	0.22
0.19	0.01	0.18	1.28	1.39	0.87	3.48	1.89	0.20	0.67	0.91	0.77	1.08
0.64	0.64	0.67	0.54	0.69	0.70	0.33	0.28	0.27	0.34	0.26	0.36	0.14
0.10	0.04	0.14	0.11	0.06	0.10	0.05	0.04	0.05	0.07	0.06	0.07	0.06
4.60	5.60	2.50	4.30	5.90	3.90	1.00	1.10	1.90	4.90	2.80	1.89	6.20
99.87	99.95	99.81	99.92	99.49	99.83	99.92	99.88	99.95	99.91	99.87	99.61	99.95
2.3	0.05	1.1	20.0	27.9	10.1	30.5	15.2	1.3	6.8	13.3	8.7	10.8
1.1	0.05	0.05	3.5	11.9	0.40	0.50	0.20	0.10	0.20	0.30	0.37	0.60
267	75	279	126	221	210	79	98	71	61	32	51	20
104	21	317	246	264	322	515	535	48	275	166	229	69
21	6	24	19	28	29	8	7	12	12	13	12	10
178	67	162	112	217	156	23	37	33	55	10	27	4
6.8	6.8	6.8	6.8			6.84	6.84	6.84	6.84	6.84	4.98	6.84
12.8	0.05	13.3	8.7	34.8	17.6	2.8	2.2	4.9	6.4	2.0	4.7	1.2
2.4	0.05	2.8	1.6	<20	<20	1.4	0.90	1.0	2.3	3.5	2.5	1.9
47	2	26	5	52	40	11	4	4	83	5	18	20
39	1	71	52	2316	64	28	23	10	144	45	57	477
14.2	1.4	15.4	14.4	17.0	13.8	10.1	8.7	9.9	10.0	12.7	9.5	4.8
14.5	14.2	20.3	22.0	36.4	32.4	45.5	35.3	35.5	32.2	40.0	33.0	28.9
1.4	1.2	0.70	1.4	0.80	0.70	2.6	2.1	1.6	1.3	1.3	1.0	1.6
0.05	0.10	0.05	0.05	0.10	0.10	0.20	0.20	0.05	0.05	0.05	0.10	0.20
61	92	58	75	53	43	204	164	115	108	129	99	87
1.9	3.2	1.7	2.8	1.7	1.3	7.0	5.1	3.7	3.3	3.8	3.3	3.4
0.90	0.20	1.7	0.20	0.20	0.30	0.60	0.20	1.7	2.0	0.40	0.22	0.50
0.50	0.50	0.50	0.50	1.0	1.0	0.50	1.0	0.50	0.50	0.50	0.99	0.50
0.05	0.05	0.05	0.05	0.10	0.10	0.05	0.05	0.05	0.20	0.05	0.06	0.05
0.70	0.40	1.9	1.3	1.0	0.40	0.70	1.3	0.20	4.7	0.70	3.9	33.0
0.20	0.20	0.20	0.40	0.10	0.20	0.70	0.50	0.30	1.1	0.40	1.0	0.10
0.50	0.90	0.50	0.80	0.50	0.30	1.6	1.2	0.60	0.70	0.70	0.62	0.40
4.8	5.8	5.2	5.8	5.4	4.0	8.7	12.5	4.5	4.8	8.0	3.8	3.4
10.5	12.5	10.8	11.9	13.2	8.8	22.0	17.0	11.5	11.9	19.2	9.4	7.6
1.6	1.9	1.8	2.0	1.9	1.7	3.6	4.6	2.1	2.1	3.2	1.6	1.5
7.8	10.2	8.8	9.1	10.4	9.2	16.0	20.1	9.3	9.9	16.1	8.9	8.4
2.4	2.6	2.5	2.8	3.2	3.6	4.6	5.2	3.4	3.1	4.5	2.8	3.0
0.71	0.84	0.93	0.87	1.2	1.5	0.74	0.78	0.75	0.74	1.2	0.67	0.38
2.7	2.6	3.3	3.4	5.0	4.8	6.1	5.4	4.4	4.1	5.9	3.6	4.2
0.44	0.41	0.57	0.61	0.91	0.98	1.1	1.0	0.82	0.76	1.1	0.65	0.67
2.8	2.8	3.7	4.1	5.4	6.7	7.5	6.3	5.3	5.2	7.6	4.9	5.2
0.58	0.52	0.77	0.79	1.2	1.4	1.7	1.4	1.3	1.2	1.5	1.2	1.0
1.7	1.7	2.2	2.8	3.2	4.2	5.3	4.3	3.9	3.6	4.9	3.6	3.3
0.24	0.24	0.33	0.38	0.46	0.67	0.83	0.69	0.64	0.59	0.75	0.63	0.55
1.7	1.9	2.2	2.8	3.0	4.7	5.7	5.1	4.2	3.9	4.6	4.0	3.9
0.22	0.28	0.35	0.44	0.46	0.66	0.86	0.71	0.66	0.63	0.79	0.65	0.64
27.6	12.0	26.0	35.4	49.7	28.5	49.1	35.5	16.3	25.7	46.8	40.6	33.3
70.4	80.8	65.5	58.0	73.2	57.9	28.6	29.0	40.4	57.8	56.9	51.8	65.7
32.6	98.5	32.6	42.5	39.3	35.6	62.0	63.4	48.6	47.7	55.4	57.1	69.6

[4] Ishikawa alteration index; AI = (100 * (K_2O + MgO)) / (K_2O + MgO + Na_2O + CaO)
[5] Chlorite-carbonate-pyrite index; CCPI = (100 * (MgO + FeO) / (MgO + FeO + Na_2O + K_2O))
[6] Advanced argillic alteration index; AAAI = (100 * SiO_2) / (SiO_2 + 10 * MgO + 10 * CaO + 10 * Na_2O)

et al., 1981; Chénard, 2006; Mueller et al., 2008; Arribas et al., 2011; Torró et al., 2013; Nelson et al., 2015). As a result, the concentrations of a number of mobile elements (e.g., Si, K, Na, Ca, Mg, Fe, Rb, Ba, Sr) are likely to have changed due to alteration. In order to assess hydrothermal alteration trends, the Ishikawa, the chlorite-carbonate-pyrite, and the advanced argillic alteration indexes (Large et al., 2001; Williams and Davidson, 2004) were calculated for each analysis (Table 1). Alteration box plots using the bivariate combination of these indexes (see Large et al., 2001; Williams and Davidson, 2004) indicate that analyzed rocks register chlorite + pyrite ± muscovite and chlorite + carbonate (i.e., propylitic), transitional muscovite + kaolinite (i.e., transitional phyllic-argillic), kaolinite + pyrophyllite (i.e., argillic), and quartz (i.e., silicic) alterations. In addition, some analyses yielded trends toward epidote and to albite alteration, likely indicating processes of cationic exchange of the hot magmas with the seawater in the seafloor (i.e., seafloor metamorphism; see Gilgen et al., 2016). Therefore, only those elements that are considered relatively immobile under mild hydrothermal alteration (high field strength elements [HFSEs], REEs, transition elements, and Th; Pearce, 2014) are used here for igneous rock classification and tectonic discrimination. To ensure the representativeness of the immobile element concentrations, rocks with geochemical evidence for changes in their masses (including both gains and losses) were discarded, resulting in the final selection of 25 whole-rock analyses (out of 51).

According to the Zr/Ti vs. Nb/Y classification diagram of Pearce (1996), compositions span from subalkaline basalts to rhyolites, with no bimodal behavior (Fig. 3). The normalized extended REE diagrams (Fig. 4) identify the host volcanic rocks of the Bayaguana area as basalts, basaltic andesites, andesites, and rhyolites. All these lithotypes show marked negative Nb and positive Th anomalies when normalized to normal mid-ocean ridge basalt (NMORB; Fig. 4A-D).

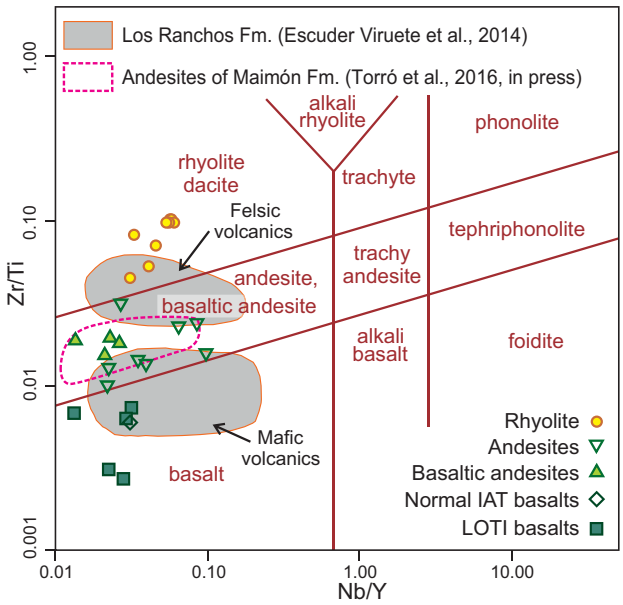

Fig. 3. Zr/Ti vs. Nb/Y classification diagram (Pearce, 1996, after Winchester and Floyd, 1977) for analyzed volcanic rocks from the Los Ranchos Formation in the Bayaguana area. Fields of mafic and felsic volcanic rocks from the Los Ranchos Formation in the Cevicos-Miches area (Escuder-Viruete et al., 2006, 2014) and intermediate volcanic rocks from the Maimón Formation (Torró et al., 2016, in press) are shown for comparison. IAT = island-arc tholeiite, LOTI = low-Ti tholeiite.

The basalts have been classified according to their TiO_2 and Cr contents (used as immobile proxy for MgO; Pearce, 2014) into low-Ti (TiO_2 < 0.8 wt %, Cr < 275 ppm) and normal (TiO_2 > 0.8 wt %, Cr < 275 ppm) island-arc tholeiitic basalts. Boninites (TiO_2 < 0.5 wt % and Cr > 275 ppm) were not detected in the study area. Studied low-Ti island-arc tholeiitic basalts (TiO_2 between 0.51 and 0.74 wt %; Cr between 6.84 and 156.26 ppm; Zr between 10.4 and 33.0 ppm) are depleted in REEs (sample/NMORB < 1; Fig. 4A, B); NMORB-normalized diagrams show near-flat segments for middle REEs (MREEs) and heavy REEs (HREEs), subtly negative to slightly positive slopes for LREEs, and an absence of Eu anomalies. Normal island-arc tholeiitic basalts (TiO_2 = 0.91 wt %; Cr = 3.51 ppm; Zr = 33.0) of the Bayaguana district show flat segments and slightly depleted values for MREEs and HREEs and negative slopes and enrichment for LREEs when normalized to NMORB. Basaltic andesites (TiO_2 between 0.52 and 0.60 wt %; Cr between 20.53 and 35.71 ppm; Zr between 56.1 and 66.2 ppm) are depleted in REEs to NMORB and have flat REE patterns in normalized diagrams (Fig. 4A, B). Mafic volcanic rocks (including basalts and basaltic andesites) show Ti/V ratios in the range of 10 to 20 and low Nb contents (<0.8 ppm; Fig. 4E, F).

Andesites (TiO_2 between 0.37 and 0.70 wt %; Cr between 6.84 and 13.68 ppm; Zr between 42.8 and 108.5 ppm) studied from the Bayaguana district present general enrichment in LREEs and both enrichment and depletion in MREEs and HREEs to NMORB. Normalized diagrams show near-flat segments for MREEs and HREEs and negative slopes for LREEs (Fig. 4C).

Rhyolites (TiO_2 between 0.14 and 0.36 wt %; Al_2O_3 between 10.44 and 12.74 wt %; Cr between 4.98 and 6.84 ppm; Zr between 87.1 and 203.7 ppm) from the Los Ranchos Formation in the Bayaguana area show near-flat to slightly LREE enriched or, in those samples with lower REE contents, even convex REE patterns (Fig. 4D). Analyzed rhyolites have negative Eu anomalies.

Hydrothermal Alteration and Mineralization

Mineralogical determinations were carried out by means of petrographic methods, scanning electron microscopy-energy dispersive spectroscopy (SEM-EDS; Quanta 200 FEI, XTE 325/D8395 equipped with an INCA Energy 250 EDS microanalysis system), and X-ray diffraction (XRD; Panalytical X'Pert PRO MPD). Petrographic features of representative samples are shown in Figures 5 and 6, and the paragenetic sequence is provided in Figure 7. The chemical compositions of minerals were determined with a five-channel JEOL JXA-8230 electron microprobe (EMP; analytical conditions described in Torró et al., 2016). All analyses were performed at the Centres Científics i Tecnològics (CCiT) of the University of Barcelona. Representative analyses on the composition of enargite and tetrahedrite group minerals are shown in Table 2.

Doña Amanda

Hydrothermal alteration in the Doña Amanda deposit produced an outer domain of propylitic altered rocks that grades

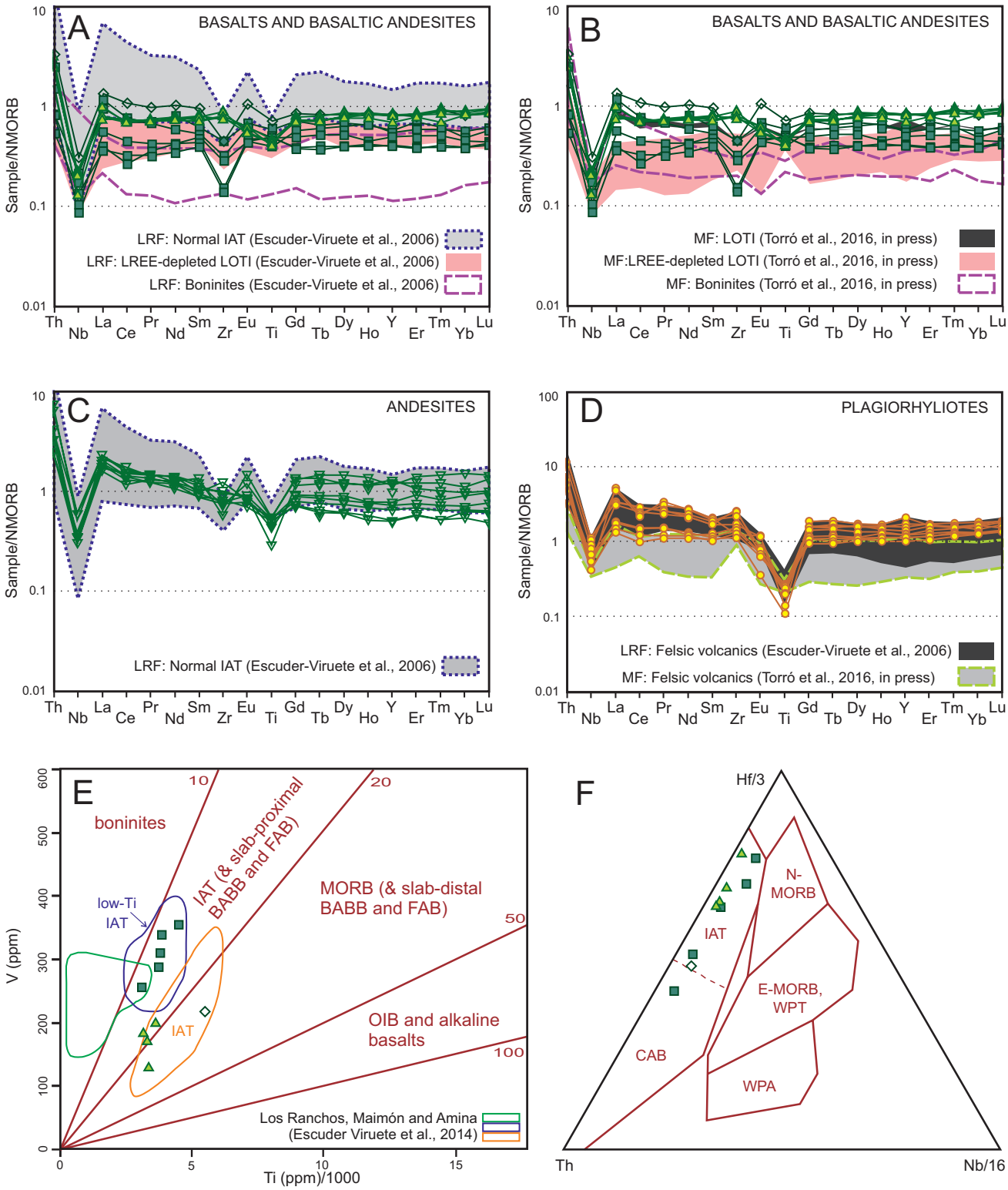

Fig. 4. Geochemical diagrams for volcanic rocks from the Los Ranchos Formation in the Bayaguana area, including compositional fields from other complexes/sources for comparison. (A-D) NMORB-normalized extended REE diagrams for the different volcanic rock types described in the main text; normalization values are after Sun and McDonough (1989). (E) Ti-V diagram (Shervais, 1982) including field nomenclature as recommended by Pearce (2014). (F) Tectonic discrimination Nb-Zr-Y diagram after Wood (1980). Symbol legend as in Figure 3. Abbreviations: BABB = back-arc basin basalt, CAB = calc-alkaline basalt, FAB = forearc basalt, IAT = island-arc tholeiite, LOTI IAT = low-Ti island-arc tholeiite, LRF = Los Ranchos Formation, MF = Maimón Formation, MORB = mid-ocean ridge basalt (N = normal, E = enriched), OIB = ocean island basalt, WPA = within-plate alkali, WPT = within-plate tholeiite.

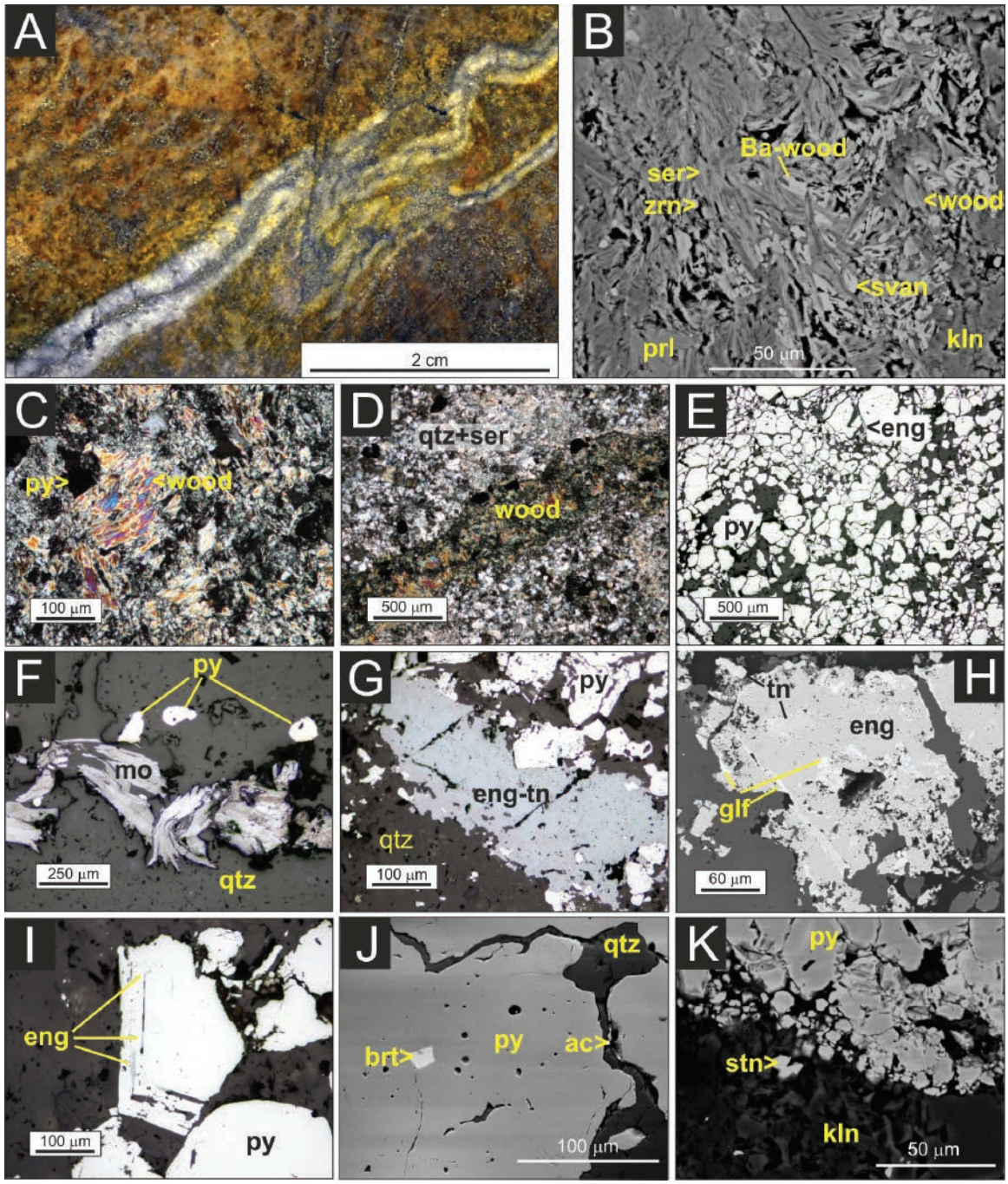

Fig. 5. Examples of Doña Amanda mineralization and hydrothermal alteration in hand sample (A) and under petrographic microscope (transmitted light, crossed polars: C, D; reflected light: E-G, I) and electron microscope (backscattered electron imaging mode: B, H, J, K). (A) Folded-sinuous quartz veins with sharply defined walls, central suture and rims of sulfides (pyrite + chalcopyrite + enargite + molybdenite), and vuggy center in a pervasively silicic and advanced argillic-altered rock with disseminations of pyrite. (B) Pervasive advanced argillic alteration of the host rock has produced kaolinite, largely recrystallized to pyrophyllite, and woodhouseite, svanbergite, and sericite. A minute hydrothermal zircon grain is also present. (C) Abundant woodhouseite, along with very fine grained quartz and scattered subeuhedral pyrite crystals, has completely replaced the original volcanic rock. (D) Pervasively silicic and phyllic altered rock cut by a vein of woodhouseite. (E) Abundant pyrite, conspicuously comminuted, in the central suture of vein shown in A; scarce enargite intergrown with quartz that has cemented pyrite grains. (F) Detail of molybdenite laths in central-sutured Cu-Mo quartz-sulfide veins. (G) Enargite and quartz have cemented subeuhedral pyrite grains in central-sutured veins. (H) Replacement of enargite and tennantite by goldfieldite. (I) Enargite has infilled elongate voids aligned parallel to crystal growth faces of euhedral pyrite crystals. (J) Minute acanthite grain in quartz cementing pyrite fragments that contain inclusions of barite. (K) Stannite crystals in kaolinite close to the contact of a pyrite vein. Abbreviations: ac = acanthite, brt = barite, eng = enargite, glf = goldfieldite, kln = kaolinite, mo = molybdenite, prl = pyrophyllite, py = pyrite, qtz = quartz, ser = sericite, stn = stannite, svan = svanbergite, tn = tennantite, wood = woodhouseite, zrn = zircon.

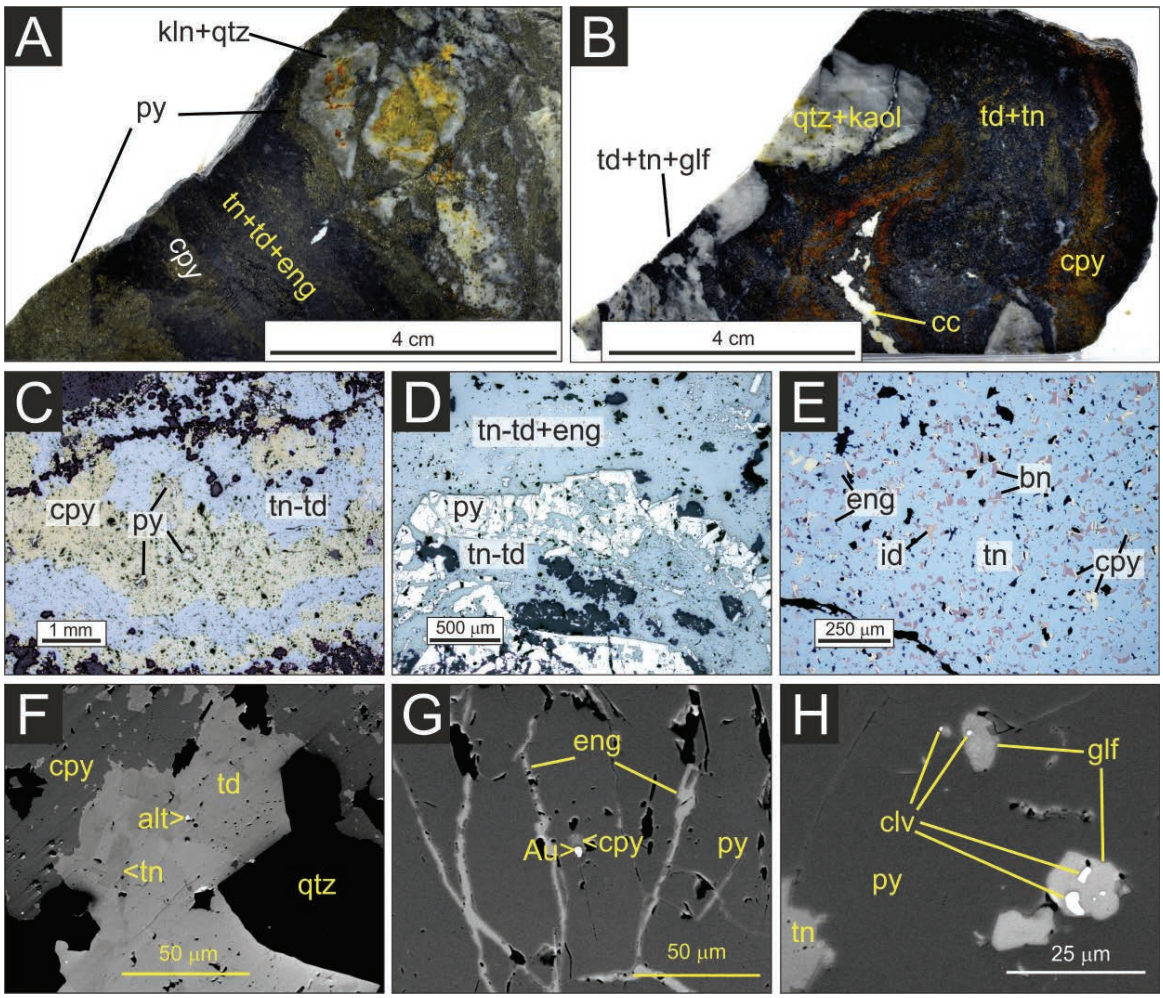

Fig. 6. Aspect of the Doña Amanda base metal mineralization in hand sample (A, B) and under petrographic (reflected light: C-E) and electron microscope (backscattered electron imaging mode: F-H). (A) Core-to-rim polished slab of zoned polymetallic vein with quartz-kaolinite-pyrite fragments cemented by pyrite grading inward to massive sulfide mineralization of tennantite-tetrahedrite, enargite, and chalcopyrite. (B) Polished slab of zoned sulfide mineralization with quartz-kaolinite fragments cemented by tetrahedrite group minerals and vein infill by layered colloform interspersed layers of tetrahedrite group minerals and chalcopyrite; cavities in the core of the vein present infill of late calcite. (C) Detail of the chalcopyrite and tennantite-tetrahedrite crusts in the sample shown in B; note the small pyrite fragments along the chalcopyrite crusts. (D) Detail of conspicuous caries textures developed on pyrite, with replacement and infilling by tennantite-tetrahedrite. Enargite is locally abundant and has been partially replaced by tennantite-tetrahedrite. (E) Complex texture in a tennantite-rich area showing replacement of bornite, enargite, and minor idaite by tennantite. Note the occurrence of exsolutions of chalcopyrite along the {100} directions of bornite. (F) Altaite grain in void of a fahlore crystal partially replaced by chalcopyrite. The original tennantite grain has been replaced by tetrahedrite. (G) Fractured and corroded pyrite crystal with infill of enargite, chalcopyrite, and native gold. (H) Corroded pyrite crystal with infill of goldfieldite and calaverite. Abbreviations: alt = altaite, Au = native gold, bn = bornite, cc = calcite, clv = calaverite, cpy = chalcopyrite, eng = enargite, glf = goldfieldite, id = idaite, kln = kaolinite, py = pyrite, qtz = quartz, td = tetrahedrite, tn = tennantite.

inward and downward to rocks that have undergone incipient phyllic alteration. This passes inward to an intermediate argillic alteration assemblage, a transitional phyllic-advanced argillic assemblage, and a silicic-altered core, the latter two with abundant sulfide disseminations. Propylitic alteration has caused chlorite alteration of pyroxene phenocrysts. The propylitically altered rocks host mm-thick veins of calcite ± quartz in the upper part of the deposit. Phyllic alteration has caused incipient replacement of plagioclase phenocrysts by fine-grained muscovite. The transitional phyllic-argillic alteration assemblage is composed primarily of kaolinite but, in the main mineralized zone, also contains pyrophyllite and several alunite supergroup minerals (Fig. 5B-D, K) that have replaced muscovite. Subhedral tabular to platy crystals of natroalunite occur as irregular replacements of woodhouseite (Fig. 5B, C). Individual platy to anhedral crystals of woodhouseite have been replaced by svanbergite and by crystals with intermediate compositions between woodhouseite and weilerite, some with Ca-rich compositions (Fig. 5B). The silicic-altered core is composed of massive quartz and, locally, vuggy quartz, with lesser amounts of alunite supergroup minerals. Silicic alteration obliterated the original mineralogy and textures of

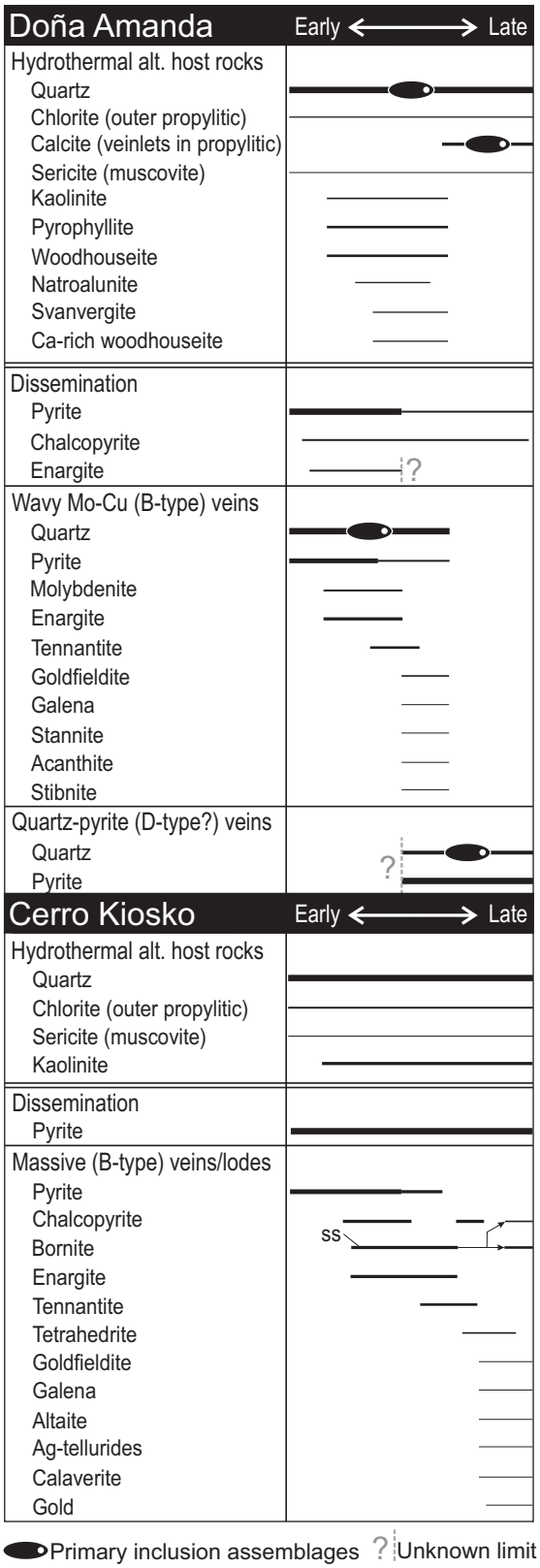

Fig. 7. Paragenetic sequence for the Doña Amanda and Cerro Kiosko hypogene mineralization and hydrothermal alteration. Width of bars approximates the abundance of minerals. The fluid inclusion symbols on the bars indicate the positions in this sequence of minerals that were used for microthermometric analyses. Abbreviation: ss = solid solution.

the rock. Quartz, kaolinite ± pyrite, and woodhouseite veins crosscut the silicic-altered core and advanced argillic alteration assemblages (Fig. 5D).

Sulfides and, to a lesser extent, sulfosalts constitute the hypogene metallic mineral association, either as disseminations or in veins. Pyrite is the dominant sulfide in disseminations (Fig. 5C), occurring as submillimeter, rounded to subangular, euhedral to subhedral grains, along with minor chalcopyrite and enargite. Pyrite is commonly fractured and variably corroded, and the fractures have been infilled by chalcopyrite, enargite, rutile, quartz, and other gangue minerals. Two sulfide-bearing vein types occur in a dense vein stockwork in the core of the deposit: (1) wavy veins of quartz with sulfide-rich central sutures and rims, sharply defined walls, and local vuggy centers (Fig. 5A), and (2) massive, planar pyrite with subordinate quartz veins (Fig. 5E). Stage 2 veins crosscut stage 1 veins. Both vein stages are surrounded by transitional phyllic-advanced argillic alteration assemblages (Fig. 5B). Stage 1 veins contain abundant pyrite and, in cores and rims, early molybdenite (Fig. 5F) and enargite (Fig. 5G), with the latter being replaced by tennantite and goldfieldite (Figs. 5H, 8; Table 2). The quartz + enargite + tennantite ± goldfieldite assemblage occurs in microfractures within pyrite and lines vugs (Fig. 5I, J), together with scant and minute galena, stannite, acanthite (Fig. 5J), and stibnite (Fig. 5K).

Cerro Kiosko

At Cerro Kiosko, an outer extensive domain of moderate-intensity propylitic alteration grades inward and downward to narrower domains of phyllic and intermediate argillic alteration. Propylitic alteration caused chlorite to replace clinopyroxenes and the glassy matrix, and produced thin veinlets of chlorite and albite alteration of plagioclase. Phyllic alteration caused fine-grained muscovite to replace plagioclase and parts of the groundmass. In intermediate argillic zones, fine-grained quartz and kaolinite pervasively altered the volcanic rocks so that no original textural features are recognizable. Fine-grained pyrite dissemination

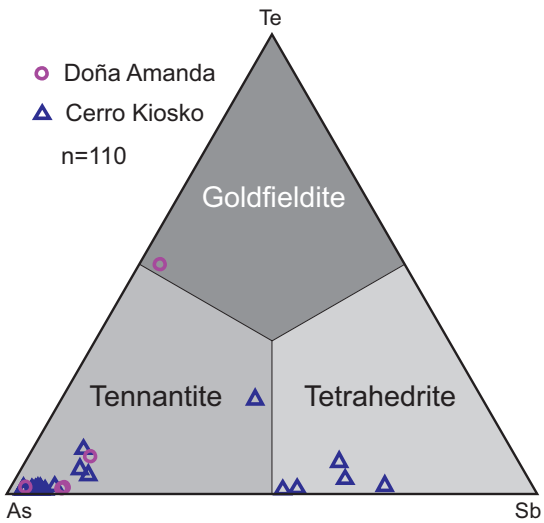

Fig. 8. Ternary classification diagram for tetrahedrite group minerals analyzed from mineralization of the Doña Amanda and Cerro Kiosko deposits according to Sb, As, and Te content.

Table 2. Chemical Composition and Structural Formulas of Selected Fahlore Minerals from the Doña Amanda and Cerro Kiosko Deposits (electron microprobe data)

Deposit	Doña Amanda							Cerro Kiosko								
Mineral	Enargite			Tennantite			Goldfieldite	Enargite			Tennantite			Tetrahedrite		
Sample no.	DA-23-10	DA-23-10	DA-23-10	DA-05-4	DA-23-10	DA-23-10	DA-23-10	OF-44-101.11A	OF-49-101.11A	OF-49-101.11A	OF-43-194.15	OF-43-194.15	OF-49-101.11A	OF-43-194.15	OF-43-194.15	OF-43-194.15
Analysis	cB 005	cB 006	cB 010	cA 005	cB 001	cB 002	cB 015	cA 010	cA 002	cC 009	cB 017	cE 021	cC 010	cB 009	cB 010	cF 003
S (wt %; d.l. = 0.02)	33.28	33.09	33.24	28.93	28.41	28.77	28.13	32.90	33.23	33.14	28.15	27.75	28.27	25.91	26.47	26.66
Fe (0.02)	0.14	0.14	0.04	0.93	0.10	0.06	0.72	0.20	0.21	0.13	6.26	5.26	3.83	4.28	4.75	4.66
Cu (0.03)	49.17	48.92	48.92	42.95	42.67	43.78	44.54	49.77	49.31	49.32	42.69	42.51	47.12	40.33	41.16	41.17
Zn (0.03)	0.07	0.07	0.09	7.51	8.18	8.28	2.50	d.l.	d.l.	d.l.	1.21	1.92	0.36	2.22	2.02	1.95
As (0.06)	17.17	16.71	17.21	19.37	16.87	17.85	8.79	16.86	17.06	17.24	15.36	13.16	15.90	4.63	6.44	7.02
Se (0.06)	0.22	0.14	0.15	0.15	0.12	0.12	d.l.	0.20	0.17	0.14	0.16	0.13	0.12	d.l.	d.l.	d.l.
Ag (0.01)	0.02	d.l.	0.02	0.02	d.l.	0.02	d.l.	0.11	d.l.	d.l.	0.04	0.06	0.02	0.12	0.13	0.11
Cd (0.07)	d.l.	d.l.	d.l.	0.11	d.l.	d.l.	0.30	d.l.	d.l.	d.l.	d.l.	0.08	d.l.	d.l.	d.l.	d.l.
Sb (0.02)	0.25	0.60	0.24	0.28	3.01	0.76	1.12	0.10	0.53	0.32	6.05	9.45	3.42	22.94	20.14	18.75
Te (0.07)	0.09	0.14	0.10	d.l.	0.21	0.46	16.19	d.l.	d.l.	d.l.	d.l.	d.l.	1.74	d.l.	d.l.	d.l.
Au (0.08)	d.l.	d.l.	d.l.	0.09	d.l.	d.l.	0.12	d.l.	d.l.	d.l.	d.l.	0.13	d.l.	d.l.	d.l.	d.l.
Hg (0.21)	d.l.	0.44	d.l.	d.l.	d.l.	d.l.	d.l.	d.l.	d.l.	0.22	d.l.	d.l.	d.l.	d.l.	d.l.	d.l.
Pb (0.12)	d.l.	d.l.	d.l.	d.l.	d.l.	d.l.	d.l.	d.l.	d.l.	d.l.	d.l.	0.14	d.l.	d.l.	d.l.	d.l.
Bi (0.06)	d.l.	d.l.	0.07	d.l.	d.l.	d.l.	0.24	d.l.	d.l.	d.l.	d.l.	d.l.	d.l.	d.l.	d.l.	0.07
Total	100.41	100.24	100.08	100.33	99.56	100.09	102.65	100.16	100.51	100.51	99.92	100.58	100.79	100.43	101.11	100.39
S (at. %)	50.62	50.63	50.73	45.71	45.73	45.69	46.49	50.24	50.54	50.47	45.31	45.18	45.14	44.78	44.82	45.15
Fe	0.13	0.12	0.04	0.85	0.09	0.05	0.68	0.18	0.18	0.12	5.79	4.92	3.51	4.25	4.62	4.53
Cu	37.74	37.77	37.67	34.24	34.66	35.09	37.14	38.35	37.85	37.90	34.68	34.93	37.97	35.17	35.17	35.18
Zn	0.05	0.05	0.07	5.82	6.46	6.45	2.03	-	-	-	0.96	1.53	0.28	1.88	1.68	1.62
As	11.18	10.94	11.24	13.10	11.62	12.13	6.22	11.02	11.11	11.24	10.58	9.17	10.87	3.42	4.67	5.09
Se	0.14	0.08	0.09	0.09	0.08	0.08	-	0.13	0.11	0.08	0.10	0.08	0.08	-	-	-
Ag	0.01	-	0.01	0.01	-	0.01	-	0.05	-	-	0.02	0.03	0.01	0.06	0.06	0.05
Cd	-	-	-	0.05	-	-	0.14	-	-	-	-	0.04	-	-	-	-
Sb	0.10	0.24	0.09	0.11	1.28	0.32	0.49	0.04	0.21	0.13	2.56	4.05	1.44	10.44	8.98	8.36
Te	0.03	0.05	0.04	-	0.09	0.18	6.72	-	-	-	-	-	0.70	-	-	-
Au	-	-	-	0.02	-	-	0.03	-	-	-	-	0.03	-	-	-	-
Hg	-	0.11	-	-	-	-	-	-	-	0.05	-	-	-	-	-	-
Pb	-	-	-	-	-	-	-	-	-	-	-	0.03	-	-	-	-
Bi	-	-	0.02	-	-	-	0.06	-	-	-	-	-	-	-	-	0.02

Note: d.l. = detection limit; Mn systematically <d.l.

increased markedly (>50% modal) along with the degree of silicic and kaolinite alteration.

Cu (± Ag ± Au) mineralization produced 0.5- to ~30-cm-thick massive sulfide stage 1 veins and lodes within strongly quartz altered host rocks. The thickest veins have multiple internal growth bands (Fig. 6). Stage 1 caused hydrofracturing of the previously altered host rocks and cementation of the fragments by pyrite (Fig. 6A). Although not common, quartz fragments are locally cemented by fahlore (Fig. 6B). Stage 2 is Cu rich (Fig. 6A, B) and consists of an initial pyrite-rich substage and a later substage with abundant Cu-bearing sulfides. Pyrite grains show evidence both of comminution, mostly along the borders of the veins, and corrosion, associated with replacement by chalcopyrite (Fig. 6C), enargite, and fahlore (Fig. 6D). The main Cu-rich substage contains chalcopyrite, bornite-idaite, and enargite, in which enargite and bornite-idaite were replaced by fahlore (Fig. 6E). The occurrence of crustiform interspersed enargite-, fahlore-, and chalcopyrite-rich mm-sized layers is common (Fig. 6B, C). In fahlore-rich layers, exsolutions of chalcopyrite along the {100} directions of bornite are conspicuous (Fig. 6E). Exsolution textures include patchy, wormy, and less abundantly coarsened cell textures (cf. Durazzo and Taylor, 1982). Fahlore is chemically heterogeneous. Tennantite has been locally altered to tetrahedrite (Fig. 8; Table 2) and a late generation of chalcopyrite (Fig. 6F). Goldfieldite, minor galena, scarce altaite (PbTe), undetermined Ag tellurides, calaverite ($AuTe_2$), and native gold (Au>>Ag) line vugs left by corrosion of tennantite and pyrite (Fig. 6F-H). Gold and calaverite grains (and Au grades) are concentrated in bornite-rich zones of the deposit. Vugs in vein cores and lodes have been filled by late calcite (Fig. 6B).

Sulfur Isotopes

The isotope composition of sulfur has been determined from 21 sulfide samples that include pure separates (n = 16) and mixtures (n = 5) from Doña Amanda (n = 8) and Cerro Kiosko (n = 13). Sulfide grains were separated by handpicking under petrographic microscope to ensure their purity. Mixtures were used only in cases where fine mineral intergrowths precluded the extraction of pure separates (not ideal, but used widely in preliminary studies; e.g., Imai, 2001). Isotopic ratios were obtained using a Delta C Finnigan MAT Delta-S mass spectrometer with an elemental analyzer at the Centres Científics i Tecnològics of the University of Barcelona. Standards for calibration were IAEA S3, IAEA S1, NBS-123, and IAEA S2. Precision of the analyses is better than ±0.2‰. Sulfur isotope compositions are expressed as the delta ‰ deviation from the Canyon Diablo Troilite standard. The obtained $\delta^{34}S$ values are summarized in Table 3 and Figure 9.

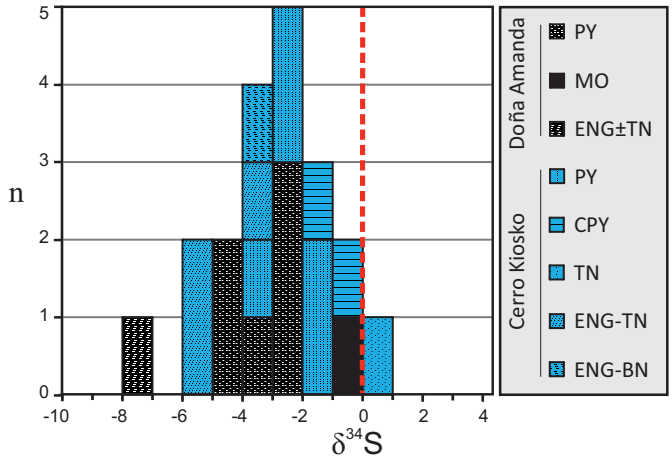

Fig. 9. Histograms showing the range of sulfur isotope data (‰, Canyon Diablo Troilite standard) for the Doña Amanda and Cerro Kiosko deposits. Abbreviations: bn = bornite, cpy = chalcopyrite, eng = enargite, mo = molybdenite, py = pyrite, tn = tennantite.

Table 3. Sulfur Isotope Compositions in Sulfides from Quartz-Sulfide Veins and Massive Sulfide Lodes in the Doña Amanda and Cerro Kiosko Deposits, Respectively

Sample no.	Deposit	Vein type	$\delta^{34}S_{py}$ (‰)	$\delta^{34}S_{cpy}$ (‰)	$\delta^{34}S_{mo}$ (‰)	$\delta^{34}S_{tn}$ (‰)	$\delta^{34}S_{eng\text{-}tn}$ (‰)	$\delta^{34}S_{eng\text{-}bn}$ (‰)
DA-05-4	Doña Amanda	B type	–2.7					
DA-23-7	Doña Amanda	B type	–4.6					
DA-23-10	Doña Amanda	B type	–2.9					
DA-23-10	Doña Amanda	B type					–7.9	
DA-23-10	Doña Amanda	B type			–0.1			
DA-23-12	Doña Amanda	B type	–4.5					
DA-23-20	Doña Amanda	B type?	–3.0					
DA-23-21	Doña Amanda	B type?	–3.8					
OF-42-72.20	Cerro Kiosko	D type	–3.0					
OF-43-194.15	Cerro Kiosko	D type				0.9		
OF-43-194.15	Cerro Kiosko	D type		–1.0				
OF-43-194.15	Cerro Kiosko	D type		–1.2				
OF-43-194.15	Cerro Kiosko	D type	–1.8					
OF-44-101.1B	Cerro Kiosko	D type	–1.9					
OF-44-101.1C	Cerro Kiosko	D type					–5.3	
OF-44-101.1C	Cerro Kiosko	D type					–5.1	
OF-49-101.1A	Cerro Kiosko	D type						–3.6
OF-49-101.11A	Cerro Kiosko	D type	–2.9					
OF-49-101.11B	Cerro Kiosko	D type					–3.6	
OF-49-101.11B	Cerro Kiosko	D type	–2.5					
OF-50-6	Cerro Kiosko	D type	–3.0					

Abbreviations: bn = bornite, cpy = chalcopyrite, eng = enargite, mo = molybdenite, tn = tennantite

In Doña Amanda, samples were selected from several wavy quartz Cu + Mo sulfide and planar pyrite ± quartz veins. $\delta^{34}S$ values range between –7.9 and –0.1‰, with a median value at –3.6‰, including six pyrite samples (–4.6 to –2.7‰), a molybdenite sample (–0.1‰), and a mixture of enargite and tennantite (–7.9‰). In Cerro Kiosko, samples were selected from massive sulfide Cu veins and lodes. $\delta^{34}S$ values range between –5.3 and +0.9‰, with a median value at –2.6‰, including six pyrite samples (–3.0 to –1.8‰), two chalcopyrite samples (–1.2 to –1.0‰), a tennantite sample (0.9‰), three mixtures of enargite and tennantite (–5.3 to –3.6‰), and a mixture of enargite and bornite (–3.6‰). Most $\delta^{34}S$ values are preferentially distributed around –2.0‰. The highest $\delta^{34}S$ values correspond to a tennantite sample from Cerro Kiosko and molybdenite from Doña Amanda. In contrast, enargite-bearing mixtures yield the lowest $\delta^{34}S$ values.

Fluid Inclusions

Petrographic and microthermometric studies of fluid inclusions were carried out on doubly polished sections (100–150 μm thick) from Doña Amanda and Cerro Kiosko (seven and three samples, respectively). In the case of Cerro Kiosko, white quartz-altered clasts, such as those shown in Figure 6A and B, were studied; however, the extremely scarce and minute (<1 μm) nature of the fluid inclusions prevented any textural observations or measurements. At Doña Amanda, fluid inclusions in calcite and quartz are scarce and small (3–15 μm in diameter). Calcite samples were obtained from centimeter-wide veins associated with propylitic-altered spilites at shallow levels to the top of the mineralized area. Primary fluid inclusions in quartz were studied in samples from quartz-sulfide veins and from the massive quartz-altered host rocks in the main mineralized zones (Fig. 5A). Only samples with no textural evidence for recrystallization of quartz were used. The analyzed primary inclusions are liquid rich (degree of filling between 0.80 and 0.98), homogenize into a liquid phase, and contain no immiscible liquids or daughter crystals (Fig. 10A, B). Fluid inclusions are negative crystal shaped or elongated, the former being much more abundant in calcite (Fig. 10B). Inclusions occur as isolated random distributions or small clusters. Evidence for necking or leakage is scant, and no other posttrapping phenomena have been observed.

Microthermometric studies on fluid inclusions from the Doña Amanda deposit were carried out using a Linkam THMSG600 heating-freezing stage. Calibration runs using synthetic fluid inclusions show that the measurements are accurate to ±0.2°C during freezing and to ±2°C during heating runs. Salinities were calculated by entering freezing point depression temperatures in the SALTY software of Bodnar et al. (1989) and Bodnar (1993). The results of microthermometric studies are summarized in Figure 10C, Table 4, and Appendix A. Inclusion fluids in quartz from stage 1 central sutured quartz-sulfide Cu-Mo veins (Fig. 5A) have homogenization temperatures (Th) between 160° and >400°C and ice melting temperatures (Tm_{ice}) between –5.0° and –12.5°C, which correspond to calculated salinities between 7.9 and 16.4 wt % NaCl equiv. Inclusions in quartz from massive sulfide planar veins (Fig. 5E) have Th between 125° and 175°C and Tm_{ice} between –2.9° and –8.4°C, which correspond to calculated salinities between 4.8 and 12.2 wt % NaCl equiv.

Table 4. Summary of Microthermometric Fluid Inclusion Data from the Doña Amanda Deposit

Sample no.	Vein type	Host	Chronology[1]	Type[2]	F high / mean / low (n)	Tm_{ice} (°C)[3] low / mean / high (n)	Tm_{clath} (°C)[4] low / mean / high (n)	Th[5] low / mean / high (n)	Mode[6]	Salinity (wt % NaCl equiv) low / mean / high
DA-23-2	Calcite	Cc	P	l-v	0.98 / 0.95 / 0.90 (21)	–9.4 / –5.1 / –3.0 (17)	0.1 / 4.7 / 15.0 (7)	119 / 142 / 162 (21)	L	5.0 / 7.9 / 13.3
DA-23-11A	Wavy, central sutured (B type)	Qtz	P	l-v	0.95 / 0.90 / 0.80 (20)	–12.5 / –8.6 / –6.0 (11)	-	190 / ? / >400 (20)	L	10.4 / 12.5 / 16.4
DA-23-11B	Wavy, central sutured (B type)	Qtz	P	l-v	0.95 / 0.94 / 0.90 (11)	–11.0 / –7.3 / –5.0 (10)	-	158 / ? / >400 (11)	L	7.9 / 10.7 / 15.0
DA-23-13B	Wavy, central sutured (B type)	Qtz	P	l-v	0.90 / 0.89 / 0.85 (6)	–8.2 / –6.7 / –5.2 (6)	-	180 / 204 / 222 (6)	L	8.1 / 10.1 / 11.9
DA-23-15	Quartz-pyrite	Qtz	P	l-v	0.95 / 0.95 / 0.90 (10)	–8.4 / –5.8 / –2.9 (9)	-	124 / 151 / 175 (10)	L	4.8 / 8.8 / 12.2
DA-23-17	Host silicification (group 1)	Qtz	P	l-v	0.95 / 0.95 / 0.95 (9)	–10.0 / –8.4 / –5.3 (9)	-	156 / 168 / 174 (9)	L	8.3 / 12.1 / 13.9
DA-23-17	Host silicification (group 2)	Qtz	P	l-v	0.95 / 0.94 / 0.90 (4)	–2.6 / –1.7 / –0.9 (4)	-	168 / 211 / 261 (4)	L	1.6 / 2.8 / 4.3

Abbreviations: Cc = calcite, Qtz = quartz
[1] P = primary
[2] l-v = liquid-vapor (liquid dominant)
[3] Final ice-melting temperature
[4] Final CO_2 clathrate dissociation temperature
[5] Temperature of homogenization
[6] Mode of homogenization; L = bubble disappearance to liquid

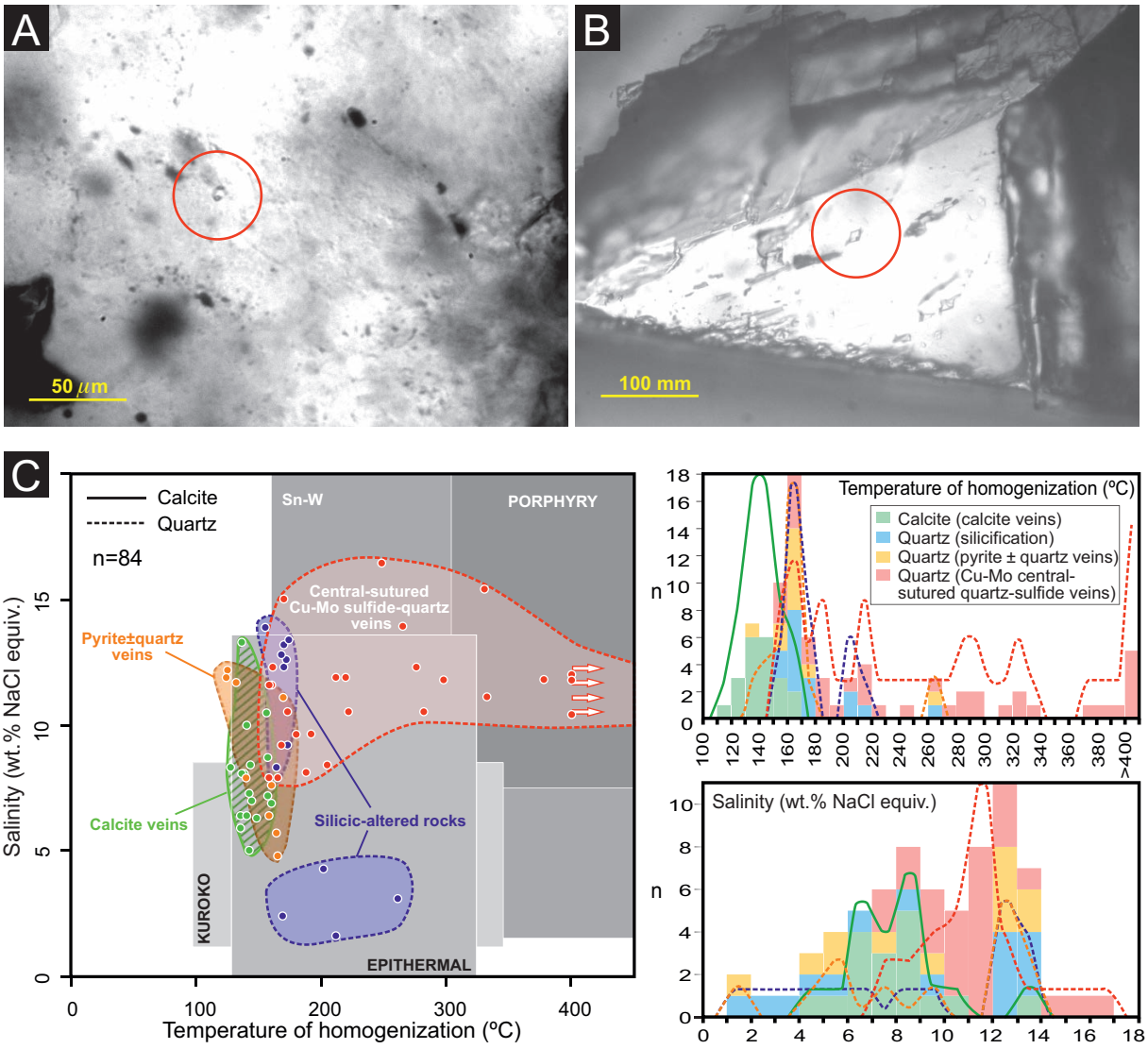

Fig. 10. (A) Photomicrograph of a primary fluid inclusion hosted in quartz in a D-type vein from Doña Amanda. (B) Photomicrograph of a primary, negative crystal-shaped fluid inclusion hosted in a calcite vein from Doña Amanda. (C) Left: Correlation between salinity and temperature of homogenization data of fluid inclusions from the Doña Amanda deposit. The position of the analyzed minerals in terms of timing of deposit formation is shown in Figure 7. Data are represented for each occurrence type as fields covering all individual measurements. These data are compared with typical ranges for inclusions from Kuroko, epithermal, Sn-W, and porphyry deposit types as compiled by Wilkinson (2001). Right: Histogram and frequency curve of temperature of homogenization (above) and salinity (below) data for fluid inclusions from the Doña Amanda deposit.

Minute and scarce inclusions found in quartz of the massively silicified hosts have Th between 152° and 261°C and Tm_{ice} values between –0.9° and –10.0°C, which correspond to calculated salinities between 1.6 and 13.9 wt % NaCl equiv. Inclusions in calcite have Th between 119° and 162°C and Tm_{ice} between –3.0 and –9.4°C, which correspond to calculated salinities between 5.0 and 13.3 wt % NaCl equiv.

Geochronology

Molybdenite Re-Os age

Molybdenite was extracted from a selected piece of drill core using a small handheld drill to create a powdered separate. The molybdenite was equilibrated with a mixed Re-double Os spike using a Carius tube dissolution (Markey et al., 2003). The double Os spike permits a correction for Os mass fractionation and will reveal any common Os. Re and Os isotope ratios were measured on a Triton TIMS machine at the AIRIE Program, Colorado State University. The analyzed molybdenite sample from the Doña Amanda deposit was collected from the DA-23-11 drill hole at a depth of 199.0 m and yielded an age of 112.6 ± 0.4 Ma. Details on analytical results are presented in Table 5.

Zircon U-Pb ages

Five rock samples from newly mapped outcrops of plagioclase-phyric rhyolite domes that intruded terrigenous and

Table 5. Re-Os Data for the Molybdenite Sample from the Doña Amanda Prospect, Bayaguana District, Dominican Republic, Along with Available Re-Os Data for Ores in the Pueblo Viejo Deposit

AIRIE Run. no.	Sample no.	Re (ppm)	± (ppm)	^{187}Os (ppb)	± (ppb)	Age, Ma (analytical error only)	Age, Ma (with ^{187}Re decay constant uncertainty)
Bayaguana							
MD-1632	DA-23-11-199.00 (mo)	1,301.9	2.2	1,537	0.5	112.6 ± 0.2	112.6 ± 0.4
Pueblo Viejo (Nelson et al., 2015)							
MD-1317	APV11-36-38.5 (mo)	6,191	10	7.276	6	112.12 ± 0.20	112.1 ± 0.4
MD-1395	APV11-39A-530.15 (mo)	105.7	1	124.1	1	112.02 ± 0.14	112.0 ± 0.4
MD-1398	APV11-40-210.75 (mo)	346.2	3	404.5	3	111.47 ± 0.12	115.5 ± 0.4
Pueblo Viejo (Kirk et al., 2014)							
	197-95.7-a (py)	8.401	0.046	0.01574	0.00013		112 ± 1
	197-95.7-b (py)	8.233	0.056	0.0156	0.00029		114 ± 2
	227-92-a (sph)	9.668	0.087	0.01927	0.00025		120 ± 2
	227-92-b (sph)	9.12	0.123	0.01809	0.00015		119 ± 2
	227-92-c (sph)	9.106	0.123	0.01762	0.00015		116 ± 2
	227-92-d (sph)	9.038	0.102	0.01809	0.00046		120 ± 3
	235-20.2-a (sph)	2.152	0.02	0.00396	0.00004		110 ± 2
	220-163.0-a (py)	4.604	0.015	0.00873	0.00012		114 ± 2

Notes: Molybdenite: Nelson et al., 2015; pyrite and sphalerite: Kirk et al., 2014; Re-Os analyses by Carius tube dissolution and equilibration with a double Os spike; analyses by NTIMS with reported uncertainties at 2σ; 5-mg sample size for both runs; common Os contents are negligible in studied molybdenite from Bayaguana; Re and Os blanks are subpicogram level and insignificant to age calculation; assumed initial ^{187}Os/^{188}Os ratio for age calculation is 0.2; age is insensitive to assumed initial Os ratio; DA-23-11 drill hole location: UTM 434561 E, 2080032 N, collar elevation

Abbreviations: mo = molybdenite, py = pyrite, sph = sphalerite

volcanogenic sedimentary rocks in the Loma Guaymarote area (equivalent to the Pueblo Viejo Member; Fig. 2B) were processed with the aim of dating their emplacement. Details of the location of the five rock samples are given in Table B1 of Appendix B. Zircon crystals were separated using panning in water. Nonmagnetic concentrates, after eliminating the magnetic fractions with a Frantz® isodynamic LB-1separator, were processed by applying the hydroseparation technique (HS) at the HS-11 laboratory of the University of Barcelona to obtain high-density mineral concentrates. The resulting nonmagnetic, high-density concentrates went through batches of acid digestion in open bombs with combinations of HF, HCl, and HNO_3. Zircons were handpicked under the binocular microscope. Once mounted and polished, zircon grains were studied by optical and cathodoluminescence (CL) imaging and analyzed for U-Pb using a sensitive high-resolution ion microprobe (SHRIMP) IIe/mc ion microprobe at the IBERSIMS Laboratory of the University of Granada, Spain. The analytical method follows that of Williams and Claesson (1987). Uranium concentration was calibrated using the SL13 reference zircon (U: 238 ppm). The U/Pb ratios were calibrated using the TEMORA-1 reference zircon (417 Ma; Black et al., 2003), which was measured every four unknowns. Common lead was corrected from the measured ^{204}Pb/^{206}Pb, using the model of terrestrial Pb evolution of Cumming and Richards (1975).

SHRIMP results and CL images of the analyzed zircons are presented in Appendix B. The extracted zircon grains are clear, colorless transparent to pale yellow translucent, stubby to square prismatic, with short pyramidal terminations and aspect ratios of ~1.5 to 2.5 and lengths of ~75 to 150 μm. CL images reveal complex oscillatory zoning in most of the zircons. Eight spot analyses on six zircon grains from sample BA-2014-1 yielded concordant ^{206}Pb/^{238}U ages that range between 122.7 ± 1.9 and 112.8 ± 2.1 Ma, with a weighted mean of 118.1 ± 2.6 Ma (mean square weighted deviation [MSWD] = 2.94; Fig. 11A). Forty-two spot analyses on 34 zircon grains from sample BA-2014-2 yielded concordant ^{206}Pb/^{238}U ages that range between 125.2 ± 2.1 and 107.6 ± 2.1 Ma, with a weighed mean of 117.2 ± 1 Ma (MSWD = 2.37, Fig. 11B). Zircon grains in sample BA-2014-4 are distinctively scarce and small (less than 75 μm long), and only nine U-Pb determinations on six zircon grains could be obtained. These are slightly discordant due to common lead, defining a poor discordia with a lower intercept age of $114.5^{+2.7}_{-3.4}$ Ma (MSWD = 1.1861; Fig. 11C); spot analysis ^{206}Pb/^{238}U ages range between 121.2 ± 2.0 and 110.9 ± 3.6 Ma (common lead uncorrected), between 120.8 ± 2.1 and 111.3 ± 4.0 Ma (^{207}Pb corrected), and between 121.9 ± 2.1 and 113.1 ± 2.6 Ma (^{208}Pb corrected). Twenty-eight spot analyses on 22 zircon grains from sample BA-2014-5 (dome with pervasive silicic alteration) yielded ^{206}Pb/^{238}U ages between 123.4 ± 4.0 and 106.5 ± 2.6 Ma, with a weighted mean of 113.4 ± 1.6 Ma (MSWD = 1.88; Fig. 11D). An inherited zircon grain, with distinctive low CL (Fig. B4), yielded a ^{206}Pb/^{238}U age of 628.2 ± 12.2 Ma. Thirty-five spot analyses on zircon grains from sample BA-2014-7 (dome with intense silicic alteration) yielded concordant ^{206}Pb/^{238}U ages between 125.8 ± 3.2 and 109.1 ± 1.7 Ma, with a weighed mean of 115.6 ± 1.1 Ma (MSWD = 2.85, Fig. 11E); an inherited zircon with remarkably low CL (Fig. B5) yielded a ^{206}Pb/^{238}U age of 277.4 ± 3.4 Ma.

Discussion

Geochemical affinities of the volcanic host rocks

Systematic marked negative Nb and positive Th anomalies to NMORB determined for all host-rock lithotypes at the

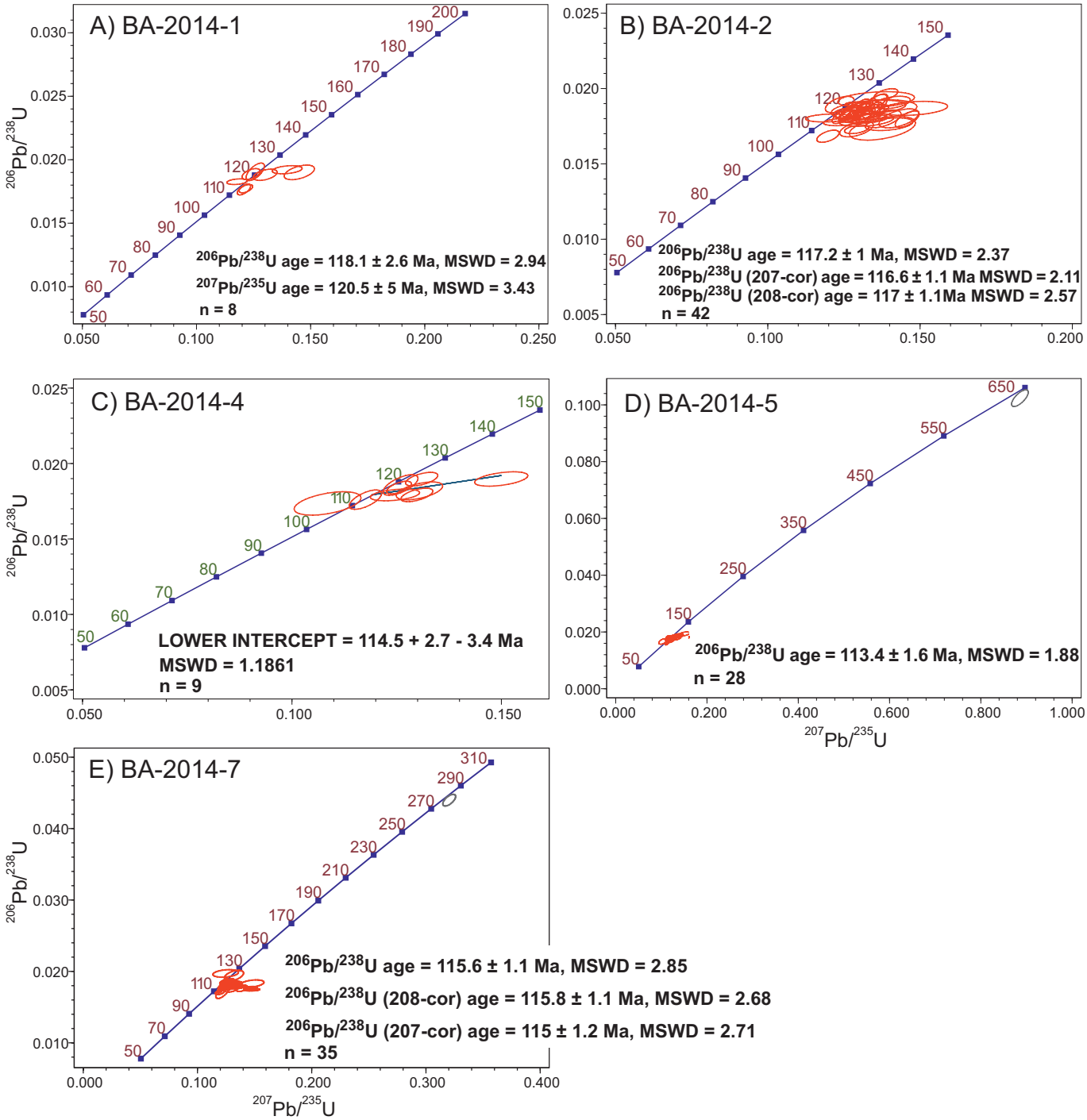

Fig. 11. Wetherill concordia plots for samples of plagioclase-phyric rhyolite domes from the Loma Guaymarote basin, eastern Bayaguana district. Gray data in D and E are not computed for age determination. MSWD = mean square weighted deviation.

Bayaguana district (Fig. 4A-D) indicate a suprasubduction zone environment for the generation of magmas and distinguish them from MORB or ocean island basalt (OIB) magmas (Pearce, 2014, and references therein). The absence of Eu anomalies in mafic volcanic rocks (including basalts and basaltic andesites) indicates that these basalts are representative of the original liquid composition. High V/Ti ratios shown by mafic volcanic rocks are indicative of formation in island-arc settings in opposition to low ratios that characterize those basalts formed in mid-ocean ridge or mature back arcs, according to the tectonic classification diagram of Shervais (1982; Fig. 4E). These ratios correspond to island-arc tholeiites and match the fields of low-Ti and normal island-arc tholeiitic basalts of primitive island-arc magmatic series in the Dominican Republic (Escuder-Viruete et al., 2014; Torró et al., 2016, in press). Further, low Nb contents (<0.8 ppm)

point to an island-arc environment in the Th-Hf-Nb discrimination diagram of Wood (1980), in which most analyses match the field of island-arc tholeiitic basalts (Fig. 4F).

No bimodal behavior was detected in the analyzed volcanic host rocks from the Bayaguana district. This is in stark contrast to strong bimodality of the Los Ranchos Formation in the Cevicos-Miches area (fig. 6 in Escuder-Viruete et al., 2006).

Boninites, not detected in the study area, were described from the base of the Los Ranchos Formation in the Cevicos-Miches area by Escuder-Viruete et al. (2006). Low-Ti island-arc tholeiitic basalts from the Bayaguana district have values and normalized patterns similar to LREE-depleted, low-Ti island-arc tholeiitic basalts described by Escuder-Viruete et al. (2006) in the lower basaltic unit of the Los Ranchos Formation in the Cevicos-Miches area, and to low-Ti island-arc tholeiitic basalts of the Maimón Formation (Torró et al., 2016, in press). In contrast, low-Ti island-arc tholeiitic basalts are enriched in REE with respect to the LREE-depleted, low-Ti island-arc tholeiitic basalts of the Maimón Formation identified by Torró et al. (2017, in press) as forearc or transitional forearc-boninite basalts (Fig. 4A, B). Normal island-arc tholeiitic basalts and basaltic andesites at Bayaguana match the field of normal island-arc tholeiitic and are enriched in REE- to LREE-depleted, low-Ti island-arc tholeiitic basalts described by Escuder-Viruete et al. (2006) in the Cevicos-Miches area. The compositions of andesites studied from the Bayaguana district are largely coincident with those of normal island-arc tholeiitic basalts described by Escuder-Viruete et al. (2006) for the mafic volcanic rocks of the upper basaltic and andesitic unit of the Los Ranchos Formation in the Cevicos-Miches area (Fig. 4C).

All analyzed rhyolites have negative Eu anomalies, suggesting fractionation in a coeval plagioclase-rich cumulate (Fig. 4D). Tholeiitic- and boninitic-like chondrite-normalized REE patterns without marked LREE enrichment and generally low REE, Zr, TiO_2, and K_2O contents are distinctive to typical calc-alkaline felsic volcanic rocks. Therefore, the studied rhyolites have tholeiitic and boninitic affinities (e.g., Lesher et al., 1986; Piercey, 2011). These values are similar to those described by Escuder-Viruete et al. (2006) and are, in general, enriched in REE with respect to felsic volcanic rocks of the Maimón Formation (Torró et al., 2016, 2017, in press). Felsic volcanic rocks in primitive island-arc series described along the Greater Antilles yield comparable lithogeochemistry and are referred to as plagiorhyolites because of the ubiquitous presence of plagioclase phenocrysts (e.g., Jolly et al., 2008, and references therein). These rocks are the extrusive counterparts of plagiogranite series intrusives generated after the anatexis of the primitive basaltic, thickened arc crust (see also Marchesi et al., 2007; Torró et al., 2017).

The new lithogeochemical data on volcanic rocks from the Los Ranchos Formation in the Bayaguana district are largely analogous to reported lithogeochemical data from the same formation in the Cevicos-Miches area (Escuder-Viruete et al., 2006). In contrast, they show systematic geochemical differences relative to volcanic rocks from the VMS-bearing Maimón Formation. This observation is on a par with the conclusions reached by Torró et al. (2017), who proposed that the two formations developed in different temporal and spatial settings during the early evolution of the Caribbean island arc. The metallogenic evolution associated with each formation was different, and these are discussed below in the framework of the general evolution of the arc system. To be noted also is that the development of argillic alteration in studied rocks, evidenced by whole-rock geochemical alteration indexes, was not detected in rocks from the Maimón Formation (Torró et al., 2016).

Evolution of the deposits and genetic model

The mineralogy of alteration and ore-bearing assemblages in the Doña Amanda and Cerro Kiosko deposits of the Bayaguana district and their structural and geometric features match those of porphyry Cu(-Mo) and high-sulfidation epithermal deposits (Simmons et al., 2005; Sillitoe, 2010). In particular, the features are similar to transitional domains between the two environments (e.g., Henley and Berger, 2011).

In Doña Amanda, Cu-Mo wavy veins of quartz with sulfide-rich central sutures and rims and sharp walls are comparable to B-type veins documented from many porphyry Cu-Mo deposits (Gustafson and Hunt, 1975; Seedorff et al., 2005; Sillitoe, 2010). Whereas Seedorff et al. (2005) describes B-type veins as veins largely lacking wall-rock alteration, Sillitoe (2010) noted the occurrence of narrow K-feldspar halos around them. Both possibilities have been documented from single deposits. At El Salvador (Chile), alteration halos rich in K-feldspar (± albite and biotite) around B-type veins are described only in deep sections of the deposit (Gustafson and Quiroga, 1995). In the absence of later deformation, the sinuosity of B-type veins at Bayaguana (Fig. 5A) is attributed to high temperatures (>400°C; Fournier, 1999) and overall quasiductile conditions. In contrast, later (i.e., D-type) veins have planar, sharp walls, consistent with formation under brittle conditions. Transitional phyllic-advanced argillic alteration halos (pyrophyllite and alunite supergroup minerals after muscovite) around B-type veins in Doña Amanda are consistent with high temperatures, as they are stable up to ~550°C (Seedorff et al., 2005; Henley and Berger, 2011). Alunite is stable at temperatures up to at least 450°C (Stoffregen et al., 1994). Temperatures of homogenization of fluid inclusions over 400°C have been determined for B-type veins from Doña Amanda, along with moderate salinities (10–17 wt % NaCl equiv; Fig. 10C). Such fluids are typical of late-stage mineralization in porphyry deposits (Fig. 10C; Redmond and Einaudi, 2010). A drastic drop in temperature (>400°–<200°C) at nearly constant salinity (with a tenuous decrease; Fig. 10C) can be explained by mixing with more dilute, cooler fluids.

In Cerro Kiosko, massive sulfide thick veins and lodes share many features with D-type veins. D veins documented from the Cavancha porphyry gold deposit (Maricunga belt, Chile; Muntean and Einaudi, 2001) have a paragenetic sequence similar to that of Cerro Kiosko, with early deposition of chalcopyrite and bornite + enargite, and late crystallization of tennantite and chalcopyrite. Evidence for open-space filling in D-type veins and lodes at Cerro Kiosko is chalcopyrite and bornite + enargite crustiform bands and, locally, vuggy cores of veins. The hypogene bornite-enargite assemblage in D veins at Cerro Kiosko marks the transition between porphyry deposits and the deepest portions of high-sulfidation deposits (ca. 500–1,000 m, but up to greater than 1,500 m; temperatures between 260° and >300°C; Hedenquist et al.,

2000; Sillitoe, 2010). Exsolution of chalcopyrite from bornite implies temperatures of formation greater than ca. 250° to 300°C at 10 to 15% chalcopyrite average in studied samples (Brett, 1964; Sugaki, 1965; Sugaki et al., 1975).

A close spatial relationship of gold with bornite-rich zones has been described in many porphyry systems (e.g., Batu Hijau and Ertsberg, Indonesia; Rubin and Kyle, 1997; Arif and Baker, 2004). In this sense, the bornite solid solution is reported to accommodate one order of magnitude more Au than intermediate solid solution (ISS, i.e., the high-temperature precursor of chalcopyrite) at a given temperature (Simon et al., 2000). Corroded pyrite grains in enargite + bornite–rich bands at Cerro Kiosko show evidence for late precipitation of native gold and calaverite along with vug lining by chalcopyrite and goldfieldite (Fig. 6G, H). We interpret these features to indicate that remobilization of Au originally hosted in bornite most probably occurred due to lower-temperature epithermal, Te-rich fluids.

Sulfur isotope data from sulfides in B- and D-type veins indicate that the dominant source of sulfur was magmatic (i.e., values near 0‰; Ohmoto and Rye, 1979). A contribution of sulfur from thermochemical reduction of sulfate in seawater is considered unlikely because no positive $\delta^{34}S$ values have been detected, as would be expected for sulfides precipitated from Lower Cretaceous seawater sulfate (~16‰; Claypool et al., 1980). The variation in $\delta^{34}S$ values could be due to slightly changing redox and/or temperature conditions (Ohmoto and Rye, 1979; Field and Fifarek, 1985), and slightly negative $\delta^{34}S$ values are also consistent with sulfide deposition from an oxidized (rich in SO_4^{2-}) magmatic fluid. Similar $\delta^{34}S$ values are reported in sulfides from high-sulfidation epithermal and related porphyry deposits (Rye et al., 1992; Hedenquist et al., 1998; Wilson et al., 2007; Cooke et al., 2011).

Pyrophyllite and alunite supergroup minerals (natroalunite, woodhouseite, and svanbergite) along with kaolinite in the Bayaguana deposits constitute hypogene argillic alteration assemblages formed at high (~400°–550°C) and intermediate to low (~200°–400°C) temperatures, respectively, which are corroborated by temperatures of homogenization of fluid inclusions. Such temperatures, plus the calculated salinities (Fig. 10C), $\delta^{34}S$ values, and hypogene sulfide assemblages are compatible with high- to intermediate-sulfidation fluids carrying magmatic sulfur within a transitional environment between a porphyry-type and a high-sulfidation epithermal deposit (Fig. 12).

Age of the rhyolite domes and mineralization

U-Pb zircon ages for the plagioclase-phyric rhyolite domes in the Bayaguana area indicate that their parental acid magmatism of tholeiitic affinity is Early Cretaceous in age (ca. 118–112 Ma; Fig. 13), which corresponds to the primitive island-arc magmatic suite in the primitive Caribbean island arc (Escuder-Viruete et al., 2014; Lidiak and Anderson, 2015). Average ages overlap, within analytical error, the reported U-Pb zircon ages for the Zambrana tonalite (Escuder-Viruete et al., 2006; Fig. 13), which intruded the Los Ranchos Formation in the Cotuí-Maimón area. They also overlap with felsic volcanic rocks from the intermediate levels of the Los Ranchos Formation, including massive quartz-feldspar porphyry rocks of the Quita Sueño Member, and also the Cotuí stock

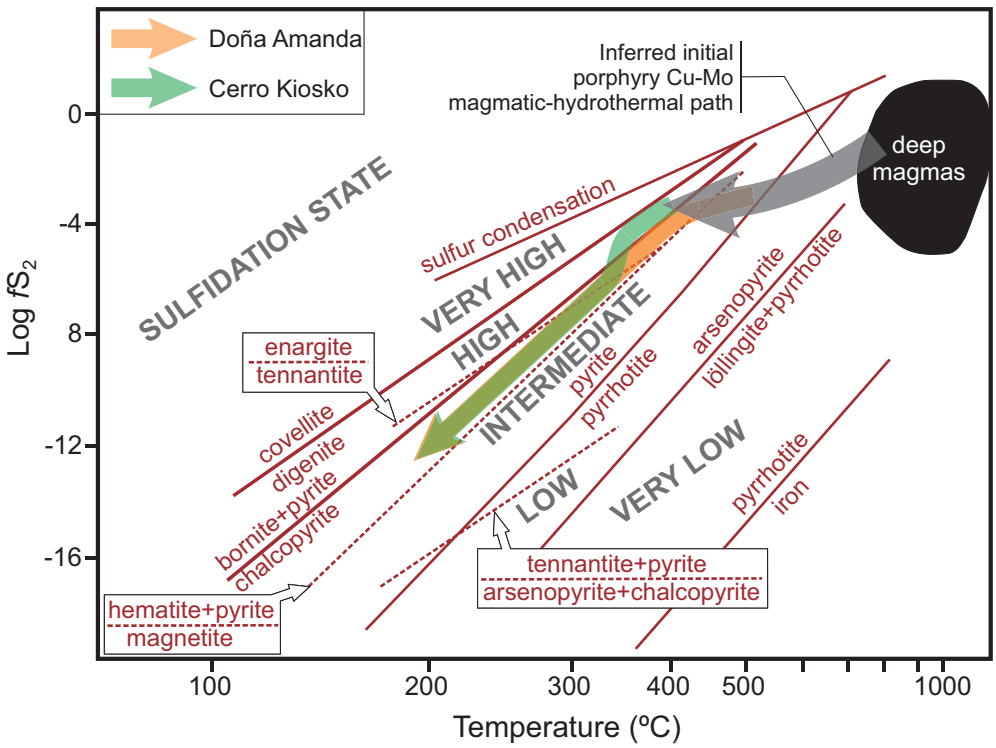

Fig. 12. Log f_{S_2} vs. T diagram, modified from Einaudi et al. (2003), illustrating the approximate cooling path of main ore stage fluids in Doña Amanda and Cerro Kiosko, based on observed mineral assemblages. Temperatures are consistent with those obtained from microthermometry of fluid inclusions.

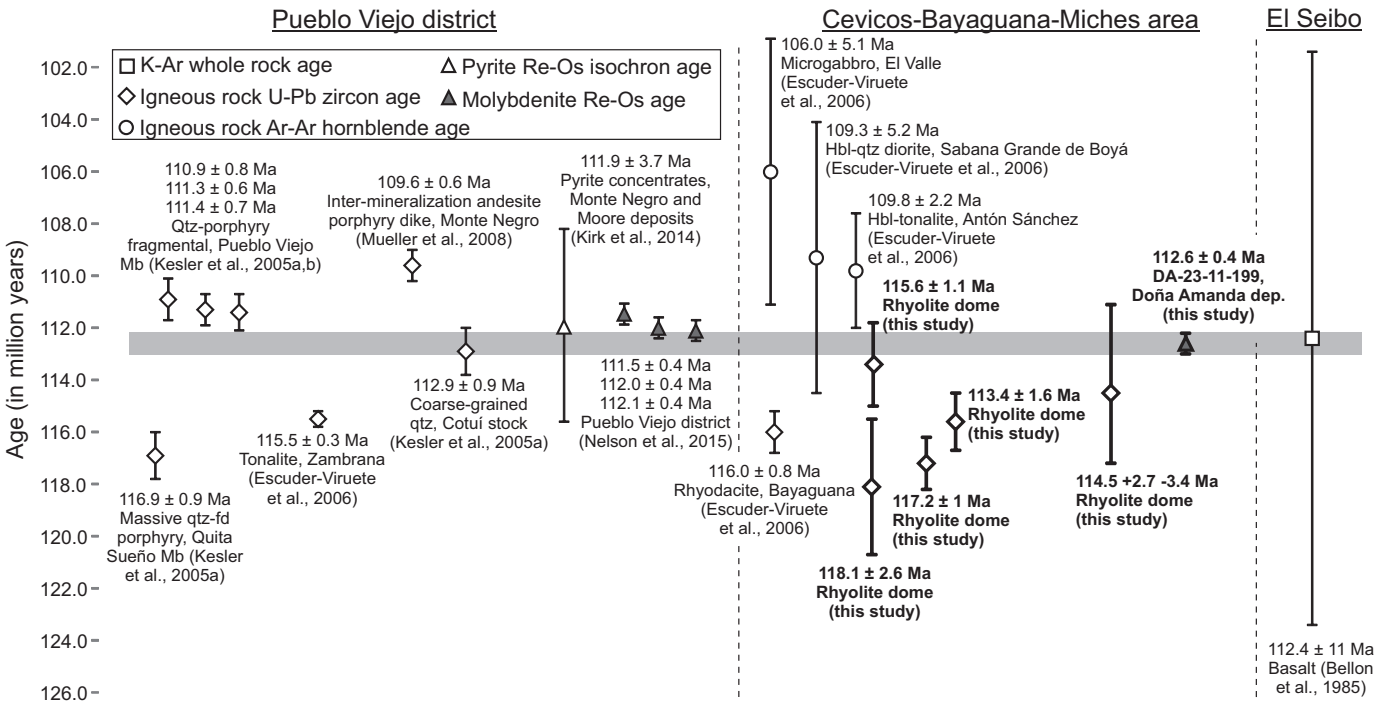

Fig. 13. Summary of age determinations on volcanic rocks from the Los Ranchos Formation (west to east: the Pueblo Viejo district, i.e., area between the road from Cotuí to Maimón and the Hatillo Reservoir; Cevicos-Bayaguana; Sierra del Seibo, close to the Samaná Bay) and ore mineralization in the Pueblo Viejo and Doña Amanda deposits. The diagram is based on literature compilation and new Re-Os molybdenite and igneous rock U-Pb zircon ages. Abbreviations: fd = feldspar, hbl = hornblende, Mb = member, qtz = quartz.

(Kesler et al., 2005a). Average U-Pb zircon ages (considering analytical errors) of the rhyolite domes are, in contrast, slightly older than those of quartz-porphyry fragmental rocks of the Pueblo Viejo Member (Kesler et al., 2005a, b) and the andesitic (intermineralization) dike in the Monte Negro pit studied by Mueller et al. (2008; Fig. 13).

A fairly large dispersion of individual spot U-Pb zircon ages was obtained. This relates to inheritance, but there are also young ages relative to the mean values and associated standard deviations (Figs. 11, 13). The prominent survival of zircon (Bindeman and Melnik, 2016) and its crystallization over what is most likely a protracted life span of large magma reservoirs underlying the mineralizing stocks (Annen, 2009) commonly result in an overall marked U-Pb age dispersion. Accordingly, the use of individual U-Pb zircon age brackets is advised to better constrain the timing of magmatic processes in subvolcanic and volcanic environments (cf. von Quadt et al., 2011). Two distinctively old inherited ages of 628 and 277 Ma likely attest to a diverse crustal input of pre-Caribbean (i.e., pre-135 Ma; Lidiak and Anderson, 2015) subducted sediments to the mantle source, as recently documented in Cuban ophiolites (cf. Rojas-Agramonte et al., 2016). Of the remaining ages that are older than average, most are between 126 and 120 Ma (Appendix A). Although oblique convergence and underthrusting of the North American plate (proto-Caribbean) beneath the Greater Antilles would have initiated around 135 Ma (Rojas-Agramonte et al., 2011; Lidiak and Anderson, 2015, and references therein), Escuder-Viruete et al. (2014) indicated that the onset of boninitic and low-Ti island-arc tholeiitic magmatism in the Hispaniola segment of the Caribbean island arc occurred at 126 Ma. Therefore, it is likely that zircons were inherited from the lower basaltic unit of the Los Ranchos Formation (Kesler et al., 1991; Escuder-Viruete et al., 2006), potentially providing a lower limit of ca. 126 Ma for Los Ranchos volcanism.

The anomalously young individual SHRIMP U-Pb zircon ages are in the range of 110 to 107 Ma—i.e., they are at least 2 m.y. younger than the lower span of average ages and corresponding errors (Fig. 13). Mueller et al. (2008) faced a similar problem when interpreting zircons ages from the intermineralization andesite dike at Pueblo Viejo. They interpreted the average age of younger zircons to correspond to the age of porphyry emplacement. In the Bayaguana area, the emplacement of rhyolitic domes probably led to the incorporation of fragments of local wall rocks (in this case, basalts and thick deposits of felsic volcanic rocks and sediments, Fig. 2B) and the consequent assimilation of their zircon. The range of ages from ~118 to 112 Ma therefore most likely constitutes the record of acid magmatism in the region (cf. Escuder-Viruete et al., 2014). The rhyolite domes were the culmination of felsic volcanism at ~110 to 107 Ma (final cooling ages at ~109–106 Ma; Escuder-Viruete et al., 2006). This proposed age range matches the age of intrusion of the intermineralization andesite dike and lateral sills observed in the Monte Negro pit at Pueblo Viejo (Fig. 13; Mueller et al., 2008) and is slightly younger than the quartz-porphyry fragmental unit at Moore (Kesler et al., 2005b). Coeval dome emplacement and deposition of the Pueblo Viejo Member sedimentary rocks (Kesler et al., 1991, 2005a, b) explain coexisting intrusive contacts and lateral changes of facies between partially reworked

dome aprons and the epiclastic sedimentary rocks (conglomerates, sandstones, siltstones, and carbonaceous mudstones) in the Loma Guaymarote area.

The Re-Os age of 112.6 ± 0.4 Ma for molybdenite in B-type veins from the Doña Amanda deposit provides evidence for the porphyry–high-sulfidation epithermal mineralizing event in the Bayaguana area to have a close temporal and genetic association with intermediate-acid magmatism. The small analytical uncertainty of this age (Fig. 13) constrains the emplacement of B-type veins prior to dome extrusion in the Loma Guaymarote basin. The strong hydrothermal alteration of the rhyolite domes, and the elevated base and precious metal tenors intercepted in basin sedimentary rocks suggest that the hydrothermal activity extended (intermittently?) for 2 to 3 m.y. This age span is not uncommon in porphyry and epithermal systems (Chiaradia et al., 2013; Holley et al., 2016). Our Re-Os age is essentially the same as Re-Os ages in pyrite concentrates (111.9 ± 3.7 Ma, Kirk et al., 2014) and molybdenite (111.5 ± 0.4, 112.0 ± 0.4, and 112.1 ± 0.4 Ma; Nelson et al., 2015) from the Pueblo Viejo district. These ages provide evidence for a regional-scale metallogenic event at 112 to 110 Ma defined by the Pueblo Viejo and Bayaguana districts.

Implications for exploration: Porphyry-epithermal vs. VMS models in the Early Cretaceous Caribbean island arc

The tendency in general studies of the metallogenic evolution of the Greater Antilles has been to link the formation of porphyry copper deposits to the Late Cretaceous calc-alkaline, mature island-arc magmatism (e.g., Hollister, 1978; Kesler et al., 1990; Proenza and Melgarejo, 1998; Nelson et al., 2011). These researchers generally considered the Pueblo Viejo deposit as a "metallogenic isolate" with no regional connection with other mineralized districts and/or particular episodes in the tectonic evolution of the Caribbean island arc. Our work demonstrates that Pueblo Viejo is part of an Early Cretaceous metallogenic belt of porphyry and high-sulfidation mineralization throughout Hispaniola.

Torró et al. (2016) pointed out the contrasting occurrence of VMS versus porphyry-epithermal mineralization in the contiguous bimodal Maimón and Los Ranchos formations, respectively. Such geologic differences correlate with slightly different tectonic settings and stages of evolution of the primitive Caribbean island arc (Torró et al., 2017). Forearc basalts, boninites, and low-Ti island-arc tholeiitic basalts of the VMS-hosting Early Cretaceous Maimón Formation (Fig. 4) indicate the establishment of a forearc environment following the initiation of W-dipping subsidence of the proto-Caribbean plate. The continued extensional regime in the overriding plate caused by slab rollback and trench migration promoted the circulation of hydrothermal fluids that led the formation of VMS deposits (cf. Ishizuka et al., 2014). Once the magmatic front and subduction angle stabilized, the generation of normal island-arc tholeiitic magmas, subaerial magmatism associated with arc crust thickening, and porphyry-epithermal mineralization took over in the intraarc zone, represented by the Los Ranchos Formation. Therefore, greenfield and brownfield exploration in the region must be accompanied by thorough characterization of the host sequences in order to better adapt the exploration strategies to targeting either VMS or porphyry-epithermal mineralization.

Conclusions

Our work reveals a transitional shallow porphyry–deep high-sulfidation epithermal environment for the deposition of ores in the Doña Amanda and Cerro Kiosko deposits of the Bayaguana district. The emplacement at 112.6 ± 0.4 Ma of Cu-Mo B-type veins demonstrates that ore deposition in the Bayaguana district coincided with primitive island-arc tholeiitic magmatism operating during the early stages of the Caribbean island-arc construction (Los Ranchos Formation). Mineralization and parental intermediate-felsic magmatism at Bayaguana were coeval with high-sulfidation epithermal Au-Ag-Cu mineralization at Pueblo Viejo, which is also hosted by the Los Ranchos Formation. This study has shown that the Bayaguana and Pueblo Viejo districts are part of the same Early Cretaceous metallogenic belt, which therefore has potential for further discoveries of porphyry and high-sulfidation deposits. The confirmed occurrence of porphyry-epithermal mineralization associated with island-arc tholeiitic volcanism in the Los Ranchos Formation highlights the exploration potential for these deposit styles in equivalent terranes of the Caribbean and elsewhere.

Acknowledgments

This research has been supported financially by Dominican project 2014-1B4-132, Spanish project CGL2012-36263, Catalan project 2014-SGR-1661, the Universities of Barcelona and Granada, an FPU Ph.D. grant to L.T. by the Ministerio de Educación of the Spanish Government, and a student research grant to L.T. from the Hugh E. McKinstry Fund of the Society of Economic Geologists. The help and hospitality extended by the Perilya-CORMIDOM staff during our field work in the Bayaguana area are also gratefully acknowledged. Ideas developed in this article on the metallogenic evolution of the Los Ranchos Formation have benefited from assistance and conversations with Hugo Domínguez. Ruth Difo is thanked for her priceless help during rock processing for zircon separation. Dr. Xavier Llovet (SCT-UB) is earnestly thanked for technical support in EMP sessions, and Dr. Marta Rejas (labGEOTOP-ICTJA-CSIC) for assistance in acid digestion runnings during the process of zircon separation. Assistance and advice on zircon separation and on SHRIMP data processing by Prof. Fernando Bea and Prof. Pilar Montero (IBERSIMS-UGR) are sincerely appreciated. This is the IBERSIMS publication nº 37. The manuscript significantly benefited from a thorough review and many constructive comments by Prof. David Cooke, Prof. Steve E. Kesler, and Dr. Isaac Corral.

REFERENCES

Aiglsperger, T., Proenza, J.A., Lewis, J.F., Labrador, M., Svojtka, M., Rojas-Purón, A., Longo, F., and Ďurišová, J., 2016, Critical metals (REE, Sc, PGE) in Ni laterites from Cuba and the Dominican Republic: Ore Geology Reviews, v. 73, p. 127–147.

Annen, C., 2009, From plutons to magma chambers: Thermal constraints on the accumulation of eruptible silicic magma in the upper crust: Earth and Planetary Science Letters, v. 284, p. 409–416.

Arif, J., and Baker, T., 2004, Gold paragenesis and chemistry at Batu Hijau, Indonesia: Implications for gold-rich porphyry copper deposits: Mineralium Deposita, v. 39, p. 523–535.

Arribas, A., Arribas, I., Draper, G., Hall, C., Kesler, S.E., McEwan, C., and Muntean, J.L., 2011, $^{40}Ar/^{39}Ar$ dating of alunite from the Pueblo Viejo gold-silver district, Dominican Republic: Economic Geology, v. 106, p. 1059–1070.

Barrick, 2015, Pueblo Viejo operations, accessed June 2015, http://www.barrick.com/operations/pueblo-viejo/default.aspx.

Bellon, H., Mecier de Lepinay, B, and Vila, J.M., 1985, Cronologie $^{40}K/^{39}Ar$ et affinités geochemiques des manifestacions magmatiques au Cretace et au Paleogene dans l'ile d'Hispaniola (Grandes Antilles): Centre National de la Recherche Scientifique, Institut Français de Recherche pour l'Exploitation de la Mer, Géodynamiques des Caraïbes Symposium, Paris, France, February 5–8, 1985, Proceedings, p. 329–339.

Bindeman, I.N., and Melnik, O.E., 2016, Zircon survival, rebirth and recycling during crustal melting, magma crystallization and mixing based on numerical modeling: Journal of Petrology, v. 57, p. 437–460.

Black, L.P., Kamo, S.L., Allen, C.M., Aleinikoff, J.A., Davis, D.W., Korsch, J.R., and Foudolis, C., 2003, TEMORA 1: A new zircon standard for Phanerozoic U-Pb geochronology: Chemical Geology, v. 200, p. 155–170.

Bodnar, R.J., 1993, Revised equation and table for determining the freezing point depression of H_2O-NaCl solutions: Geochimica et Cosmochimica Acta, v. 57, p. 683–684.

Bodnar, R.J., Sterner, S.M., and Hall, D.L., 1989, SALTY: A FORTRAN program to calculate compositions of fluid inclusions in the system NaCl-KCl-H_2O: Computers and Geosciences, v. 15, p. 19–41.

Boschman, L.M., van Hinsbergen, D.J.J., Torsvik, T.H., Spakman, W., and Pindell, J.L., 2014, Kinematic reconstruction of the Caribbean region since the Early Jurassic: Earth-Science Reviews, v. 138, p. 102–136.

Bowin, C.O., 1966, Geology of the central Dominican Republic: Geological Society of America Memoirs, v. 98, p. 11–84.

Brett, P.R., 1964, Experimental data from the system Cu-Fe-S and their bearing on exsolution textures in ores: Economic Geology, v. 59, p. 1241–1269.

Chénard, D., 2006, Evaluation of seven projects in the Dominican Republic: Santo Domingo, Technical Report to Globestar Mining and Corporación Minera Dominicana S.A., 53 p.

Chiaradia, M., Schaltegger, U., Spikings, R., Wotzlaw, J.F., and Ovtcharova, M., 2013, How accurately can we date the duration of magmatic-hydrothermal events in porphyry systems?—an invited paper: Economic Geology, v. 108, p. 565–584.

Claypool, G.E., Holser, W.T., Kaplan, I.R., Sakai, H., and Zak, I., 1980, The age curves for sulfur and oxygen isotopes in marine sulfate and their mutual interpretation: Chemical Geology, v. 28, p. 199–260.

Cooke, D.R., Deyell, C.L., Waters, P.J., Gonzales, R.I., and Zaw, K., 2011, Evidence for magmatic-hydrothermal fluids and ore-forming processes in epithermal and porphyry deposits of the Baguio district, Philippines: Economic Geology, v. 106, p. 1399–1424.

Cumming, G.L., and Kesler, S.E., 1987, Lead isotopic composition of the oldest volcanic rocks of the eastern Greater Antilles island arc: Chemical Geology, v. 65, p. 15–23.

Cumming, G.L., and Richards, J.R., 1975, Ore lead isotope ratios in a continuously changing Earth: Earth and Planetary Science Letters, v. 28, p. 155–171.

Cumming, G.L., Kesler, S.E., and Krstic, D., 1982, Source of lead in sulfide ore at the Pueblo Viejo gold-silver oxide deposit, Dominican Republic: Economic Geology, v. 77, p. 1939–1941.

Durazzo, A., and Taylor, L.A., 1982, Experimental exsolution textures in the system bornite-chalcopyrite: Genetic implication concerning natural ores: Mineralium Deposita, v. 79, p. 79–97.

Einaudi, M.T., Hedenquist, J.W., and Inan, E., 2003, Sulfidation state of fluids in active and extinct hydrothermal systems: Transitions from porphyry to epithermal environments: Society of Economic Geologists, Special Publication, no. 10, p. 285–313.

Escuder-Viruete, J., Díaz de Neira, A., Hernaiz Huerta, P.P., Monthel, J., García-Senz, J., Joubert, M., Lopera, E., Ullrich, T., Friedman, R., Mortensen, D., and Pérez-Estaún, A., 2006, Magmatic relationships and ages of Caribbean island arc tholeiites, boninites and related felsic rocks, Dominican Republic: Lithos, v. 90, p. 161–186.

Escuder-Viruete, J., Díaz de Neira, A., Hernaiz Huerta, P.P., García-Senz, J., Monthel, J., Joubert, M., Lopera, E., Ullrich, T., Friedman, R., Weis, D., and Pérez-Estaún, A., 2007, Implicaciones tectonomagmáticas y edad de las toleítas de arco-isla, boninitas y rocas ácidas relacionadas de la formación Los Ranchos, Cordillera Oriental, República Dominicana: Boletín Geológico y Minero, v. 118, p. 195–220.

Escuder-Viruete, J., Joubert, M., Urien, P., Friedman, R., Weis, D., Ullrich, T., and Pérez-Estaún, A., 2008, Caribbean island-arc rifting and back-arc basin development in the Late Cretaceous: Geochemical, isotopic and geochronological evidence from Central Hispaniola: Lithos, v. 104, p. 378–404.

Escuder-Viruete, J., Castillo Carrión, M., and Pérez-Estaún, A., 2014, Magmatic relationships between depleted mantle harzburgites, boninitic cumulate gabbros and subduction related tholeiitic basalts in the Puerto Plata ophiolitic complex, Dominican Republic: Implications for the birth of the Caribbean island-arc: Lithos, v. 196–197, p. 261–280.

Field, C.W., and Fifarek, R.H., 1985, Light stable-isotope systematics in the epithermal environment: Reviews in Economic Geology, v. 2, p. 99–128.

Fournier, R.O., 1999, Hydrothermal processes related to movement of fluid from plastic into brittle rock in the magmatic-epithermal environment: Economic Geology, v. 94, p. 1193–1211.

Gilgen, S.A., Diamond, L.W., and Mercolli, I., 2016, Sub-seafloor epidosite alteration: Timing, depth and stratigraphic distribution in the Semail ophiolite, Oman: Lithos, v. 260, p. 191–210.

GoldQuest, 2015, Romero project overview, accessed June 2015, http://www.goldquestcorp.com/index.php/projects/romero-project/romero-overview.

Gustafson, L.B., and Hunt, J.P., 1975, The porphyry copper deposit at El Salvador, Chile: Economic Geology, v. 70, p. 857–912.

Gustafson, L.B., and Quiroga, J., 1995, Patterns of mineralization and alteration below the porphyry copper orebody at El Salvador, Chile: Economic Geology, v. 90, p. 2–16.

Hedenquist, J.W., Arribas, Jr., A., and Reynolds, T.J., 1998, Evolution of an intrusion-centered hydrothermal system: Far Southeast-Lepanto porphyry and epithermal Cu-Au deposits, Philippines: Economic Geology, v. 93, p. 373–404.

Hedenquist, J.W., Arribas, A., and Gonzalez-Urien, E., 2000, Exploration for epithermal gold deposits: Reviews in Economic Geology, v. 13, p. 245–277.

Henley, R.W., and Berger, B.R., 2011, Magmatic-vapor expansion and the formation of high-sulfidation gold deposits: Chemical controls on alteration and mineralization: Ore Geology Reviews, v. 39, p. 63–74.

Holley, E.A., Bissig, T., and Monecke, T., 2016, The Veladero high-sulfidation epithermal gold deposit, El Indio-Pascua belt, Argentina: Geochronology of alunite and jarosite: Economic Geology, v. 111, p. 311–330.

Hollister, V.F., 1978, Porphyry copper deposits of the Caribbean, *in* Hollister, V.F., ed., Geology of the porphyry copper deposits of the Western Hemisphere: New York, Society of Mining Engineers, American Institute of Mining, Metallurgical and Petroleum Engineers, p. 149–157.

Imai, A., 2001, Generation and evolution of ore fluids for porphyry Cu-Au mineralization of the Santo Tomas II (Philex) deposit, Philippines: Resource Geology, v. 51, p. 71–96.

Ishizuka, O., Umino, S., Taylor, R.N., and Kanayama, K., 2014, Evidence for hydrothermal activity in the earliest stages of intraoceanic arc formation: Implications for ophiolite-hosted hydrothermal activity: Economic Geology, v. 109, p. 2159–2178.

Jolly, W.T., Lidiak, E.G., and Dickin, A.P., 2008, The case for persistent southwest-dipping Cretaceous convergence in the northeast Antilles: Geochemistry, melting models, and tectonic implications: Geological Society of America Bulletin, v. 120, p. 1036–1052.

Kesler, S.E., Russell, N., Seaward, M., Rivera, J., McCurdy, K., Cumming, G.L., and Sutter, J.F., 1981, Geology and geochemistry of sulfide mineralization underlying the Pueblo Viejo gold-silver oxide deposit, Dominican Republic: Economic Geology, v. 76, p. 1096–1117.

Kesler, S.E., Levy, E., and Martín, C., 1990, Metallogenic evolution of the Caribbean region, *in* Dengo, G., and Case, J.E., eds., The Caribbean region: The geology of North America: Geological Society of America, v. H, p. 77–140.

Kesler, S.E., Russell, N., Polanco, J., McCurdy, K., and Cumming, G.L., 1991, Geology and geochemistry of the Early Cretaceous Los Ranchos Formation, central Dominican Republic: Geological Society of America Special Paper, v. 262, p. 187–201.

Kesler, S.E., Campbell, I.H., and Allen, C.M., 2005a, Age of the Los Ranchos Formation, Dominican Republic: Timing and tectonic setting of primitive island arc volcanism in the Caribbean region: Geological Society of America Bulletin, v. 117, p. 987–995.

Kesler, S.E., Campbell, I.H., Smith, C.N., Hall, C.M., and Allen, C.M., 2005b, Age of the Pueblo Viejo gold-silver deposit and its significance to models for high-sulfidation epithermal mineralization: Economic Geology, v. 100, p. 253–272.

Kirk, J.D., Ruiz, J., Kesler, S.E., Simon, A., and Muntean, J.L., 2014, Re-Os age of the Pueblo Viejo epithermal deposit, Dominican Republic: Economic Geology, v. 109, p. 503–512.

Large, R.R., Gemmell, J.B., Paulick, H., and Huston, D., 2001, The alteration box plot: A simple approach to understanding the relationships between

alteration mineralogy and lithogeochemistry associated with volcanic-hosted massive sulfide deposits: Economic Geology, v. 96, p. 957–971.
Lesher, C.M., Gibson, H.L., and Campbell, I.H., 1986, Composition-volume changes during hydrothermal alteration of andesite at Buttercup Hill, Noranda district, Quebec: Geochimica et Cosmochimica Acta, v. 50, p. 2693–2705.
Lewis, J.F., and Draper, G., 1990, Geology and tectonic evolution of the northern Caribbean margin, *in* Dengo, G., and Case, J.E., eds., The Caribbean region. The geology of North America, v. H: Boulder, Geological Society of America, p. 77–140.
Lewis, J.F., Astacio, V.A., Espaillat, J., and Jiménez, J., 2000, The occurrence of volcanogenic massive sulfide deposits in the Maimón Formation, Dominican Republic: The Cerro de Maimón, Loma Pesada and Loma Barbuito deposits: Geological Society of Canada Special Publication, v. 2, p. 213–239.
Lewis, J.F., Escuder Viruete, J., Hernaiz Huerta, P.P., Gutiérrez, G., and Draper, G., 2002, Subdivisión geoquímica del arco de isla Circum-Caribeño, Cordillera Central Dominicana: Implicaciones para la formación, acreción y crecimiento cortical en un ambiente intraoceánico: Acta Geologica Hispanica, v. 37, p. 81–122.
Lidiak, E.G., and Anderson, T.H., 2015, Evolution of the Caribbean plate and origin of the Gulf of Mexico in light of plate motions accommodated by strike-slip faulting: Geological Society of America Special Paper, v. 513, p. SPE513–01.
Mann, P., Draper, G., and Lewis, J.F., 1991, An overview of the geologic and tectonic development of Española: Geological Society of America Special Paper, v. 262, p. 1–28.
Marchesi, C., Garrido, C.J., Bosch, D., Proenza, J.A., Gervilla, F., Monié, P., and Rodríguez-Vega, A., 2007, Geochemistry of Cretaceous magmatism in eastern Cuba: Recycling of North American continental sediments and implications for subduction polarity in the Greater Antilles: Journal of Petrology, v. 48, p. 1813–1840.
Marchesi, C., Garrido, C.J., Proenza, J.A., Hidas, K., Butjosa, L., and Lewis, J.F., 2016, Geochemical record of subduction initiation in the sub-arc mantle: Insights from Loma Caribe peridotite (Dominican Republic): Lithos, v. 252–253, p. 1–15.
Markey, R.J., Hannah, J.L., Morgan, J.W., and Stein, H.J., 2003, A double spike for osmium analysis of highly radiogenic samples: Chemical Geology, v. 200, p. 395–406.
Mueller, A.G., Hall, G.C., Nemchin, A.A., and O'Brien, D., 2008, Chronology of the Pueblo Viejo epithermal gold-silver deposit, Dominican Republic: Formation in an Early Cretaceous intraoceanic island arc and burial under ophiolite: Mineralium Deposita, v. 43, p. 873–890.
Muntean, J.L., and Einaudi, M.T., 2001, Porphyry-epithermal transition: Maricunga belt, northern Chile: Economic Geology, v. 96, p. 743–772.
Myczynski, R., and Iturralde-Vinent, M., 2005, The late lower Albian invertebrate fauna of the Rio Hatillo Formation of Pueblo Viejo, Dominican Republic: Caribbean Journal of Science, v. 41, p. 782–796.
Nelson, C.E., 2000, Volcanic domes and gold mineralization in the Pueblo Viejo district, Dominican Republic: Mineralium Deposita, v. 35, p. 511–525.
Nelson, C.E., Proenza, J.A., Lewis, J.F., and López-Kramer, J., 2011, The metallogenic evolution of the Greater Antilles: Geologica Acta, v. 9, p. 229–264.
Nelson, C.E., Stein, H.J., Dominguez, H., Carrasco, C., Barrie, T., Torró, L., and Proenza, J., 2015, Re-Os dating of molybdenite from the Pueblo Viejo Au-Ag-Cu and Douvray Cu-Au districts, Hispaniola: Economic Geology, v. 110, p. 1101–1110.
Ohmoto, H., and Rye, R.O., 1979, Isotopes of sulfur and carbon, *in* Barnes, H.L., ed., Geochemistry of hydrothermal ore deposits, 2nd edition: New York, Wiley, p. 491–559.
Pearce, J.A., 1996, A user's guide to basalt discrimination diagrams: Geological Association of Canada, Special Publication 12, p. 79–113.
——2014, Immobile elements fingerprinting of ophiolites: Elements, v. 10, p. 101–108.
Perilya, 2015, Bayaguana concessions, accessed June 2015, http://www.perilya.com.au/our-business/exploration/dominican/bayaguana-concessions.
Piercey, S.J., 2011, The setting, style, and role of magmatism in the formation of volcanogenic massive sulfide deposits: Mineralium Deposita, v. 46, p. 449–471.
Proenza, J.A., and Melgarejo, J.C., 1998, Una introdución a la metalogenia de Cuba bajo la perspectiva de la tectónica de placas: Acta Geologica Hispanica, v. 33, p. 89–132.
Redmond, P.B., and Einaudi, M.T., 2010, The Bingham Canyon porphyry Cu-Mo-Au deposit. I. Sequence of intrusions, vein formation, and sulfide deposition: Economic Geology, v. 105, p. 43–68.
Redwood, S., 2014, Dominican Republic. Gold surge: Mining Journal, http://www.mining-journal.com/world/centralsouth-america/dominican-republic-gold-surge.
——2015, Dominican Republic on the mining map: Mining Journal, http://www.mining-journal.com/world/centralsouth-america/dominican-republic-on-the-mining-map.
Rojas-Agramonte, Y., Kröner, A., García-Casco, A., Somin, M., Iturralde-Vinent, M., Mattison, J.M., Millán Trujillo, G., Sukar, K., Pérez Rodríguez, M., Carrasquilla, M., Wingate, M., and Liu, D., 2011, Timing and evolution of Cretaceous island arc magmatism in central Cuba: Implications for the history of arc systems in the northwestern Caribbean: Journal of Geology, v. 119, p. 619–640.
Rojas-Agramonte, Y., Garcia-Casco, A., Kemp, A., Kröner, A., Proenza, J.A., Lázaro, C., and Liu, D., 2016, Recycling and transport of continental material through the mantle wedge above subduction zones: A Caribbean example: Earth and Planetary Science Letters, v. 436, p. 93–107.
Román-Alday, M.C., Torró, L., Proenza, J.A., Melgarejo, J.C., Romero, J., Amarante, A., Espaillat, J., and Nelson, C., 2015, The Romero Cu-Au-Zn deposits, Cordillera Central, Dominican Republic: Preliminary data on the mineralogy and geochemistry of mineralization: Society for Geology Applied to Mineral Deposits, Biennial SGA Meeting, 13th, Nancy, France, v. 55, Proceedings, p. 2087–2090.
Rubin, J.N., and Kyle, J.R., 1997, Precious metal distribution in porphyry-, skarn-, and replacement-type ore deposits of the Ertsberg (Gunung Bijih) district, Irian Jaya, Indonesia: Economic Geology, v. 92, p. 535–550.
Russell, N., and Kesler, S.E., 1991, Geology of the maar-diatreme complex hosting precious metal mineralization at Pueblo Viejo, Dominican Republic: Geological Society of America, Special Paper 262, p. 203–215.
Rye, R.O., Bethke, P.M., and Wasserman, M.D., 1992, The stable isotope geochemistry of acid sulfate alteration: Economic Geology, v. 87, p. 225–262.
Seedorff, E., Dilles, J.H., Proffett, J.M., Einaudi, M.T., Zurcher, L., Stavast, W.J.A., Johnson, D.A., and Barton, M.D., 2005, Porphyry deposits: Characteristics and origin of hypogene features: Economic Geology 100th Anniversary Volume, p. 251–298.
Shervais, J.W., 1982, Ti-V plots and the petrogenesis of modern and ophiolitic lavas: Earth and Planetary Science Letters, v. 59, p. 101–118.
Sillitoe, R.H., 2010, Porphyry copper systems: Economic Geology, v. 105, p. 3–41.
Sillitoe, R.H., Hall, D.J., Redwood, S.D., and Waddell, A., 2006, Pueblo Viejo high sulfidation epithermal gold-silver deposit, Dominican Republic: A new model of formation beneath barren limestone cover: Economic Geology, v. 101, p. 1427–1435.
——2007, Pueblo Viejo high-sulfidation epithermal gold-silver deposit, Dominican Republic: A new model of formation beneath barren limestone cover—a reply: Economic Geology, v. 102, p. 758–760.
Simmons, S.F., White, N.C., and John, D.A., 2005, Geological characteristics of epithermal precious and base metal deposits: Economic Geology 100th Anniversary Volume, p. 485–522.
Simon, G., Kesler, S.E., Essene, E.J., and Chryssoulis, S.L., 2000, Gold in porphyry copper deposits: Experimental determination of the distribution of gold in the Cu-Fe-S system at 400° to 700°C: Economic Geology, v. 95, p. 259–270.
Smiley, C.J., 2002, Lower Cretaceous plants from the Dominican Republic: Department of Geology and Geography, University of the West Indies, Caribbean Geological Conference, 15th, Kingston, Jamaica, 1998, Proceedings, p. 119–129.
Stoffregen, R.E., Rye, R.O., and Wasserman, M.D., 1994, Experimental studies of alunite: I. ^{18}O-^{16}O and D-H fractionation factors between alunite and water at 250–450°C: Geochimica et Cosmochimica Acta, v. 58, p. 903–916.
Sugaki, A., 1965, Studies on the join Cu_5FeS_4-$CuFeS_{2-x}$ as geothermometer: Journal of Japanese Association of Mineralogists, Petrologists and Economic Geologists, v. 53, p. 1–17.
Sugaki, A., Shima, H., Kitakaze, A., and Harada, H., 1975, Isothermal phase relations in the system Cu-Fe-S under hydrothermal conditions at 350°C and 300°C: Economic Geology, v. 70, p. 806–823.
Sun, S.S., and McDonough, W.F., 1989, Chemical and isotopic systematics of oceanic basalts: Implication for mantle composition and processes: Geological Society London Special Publications, v. 42, p. 313–345.
Toloczyki, M., and Ramirez, I., 1991, Geologic map of the Dominican Republic 1:250,000: Ministry of Industry and Commerce, Department of Mining, Geographic Institute of the University of Santo Domingo.
Torró, L., Proenza, J.A., Melgarejo, J.C., Carrasco, C.A., Domínguez, H.S., Nelson, C., and Lewis, J.F., 2013, Alteration mineral domains under Loma

la Cuaba: New insights as to the origin of the mineralization in the Pueblo Viejo district: Society for Geology Applied to Mineral Deposits, SGA Biennial Meeting, 12th, Uppsala, Sweden, 2013, Extended Abstracts, v. 2, p. 590–593.

Torró, L., Proenza, J.A., Melgarejo, J.C., Alfonso, P., Farré de Pablo, J., Colomer, J.M., García-Casco, A., Gubern, A., Gallardo, E., Cazañas, X., Chávez, C., del Carpio, R., León, P., Nelson, C., and Lewis, J.F., 2016, Mineralogy, geochemistry and sulfur isotope characterization of the Cerro de Maimón (Dominican Republic), San Fernando and Antonio (Cuba): Lower Cretaceous VMS deposits associated to the subduction initiation of the Proto-Caribbean lithosphere within a fore-arc: Ore Geology Reviews, v. 72, p. 794–817.

Torró, L., Proenza, J.A., Marchesi, C., García-Casco, A., and Lewis, J.F., 2017, Petrogenesis of meta-volcanic rocks from the Maimón Formation (Dominican Republic): Geochemical record of the nascent Greater Antilles paleo-arc: Lithos, v. 278–281, p. 255–273.

Torró, L., Proenza, J.A., García-Casco, A., Farré de Pablo, J., del Carpio, R., León, P., Chávez, C., Domínguez, H., Brower, S., Espaillat, J., Nelson, C.E., and Lewis, J.F., in press, La geoquímica de la Formación Maimón (Cordillera Central, República Dominicana) revisada: Boletín Geológico y Minero, in press.

Unigold, 2015, Neita concession, accessed June 2015, http://www.unigoldinc.com/s/neita.asp.

von Quadt, A., Erni, M., Martinek, K., Moll, M., Peytcheva, I., and Heinrich, C.A., 2011, Zircon crystallization and the lifetimes of ore-forming magmatic-hydrothermal systems: Geology, v. 39, p. 731–734.

Wilkinson, J.J., 2001, Fluid inclusions in hydrothermal ore deposits: Lithos, v. 55, p. 229–272.

Williams, I.S., and Claesson, S., 1987, Isotopic evidence for the Precambrian provenance and Caledonian metamorphism of high grade paragneisses from the Seve Nappes, Scandinavian Caledonides. II: Ion microprobe zircon U-Th-Pb: Contribution to Mineralogy and Petrology, v. 97, p. 205–217.

Williams, N.C., and Davidson, G.J., 2004, Possible submarine advanced argillic alteration at the Basin Lake prospect, western Tasmania, Australia: Economic Geology, v. 99, p. 987–1002.

Wilson, A.J., Cooke, D.R., Harper, B.J., and Deyell, C.L., 2007, Sulfur zonation in the Cadia district, southeastern Australia: Exploration significance and implications for the genesis of alkali porphyry gold-copper deposits: Mineralium Deposita, v. 42, p. 465–487.

Winchester, J.A., and Floyd, P.A., 1977, Geochemical discrimination of different magma series and their differentiation products using immobile elements: Chemical Geology, v. 20, p. 325–343.

Wood, D.A., 1980, The application of a Th-Hf-Ta diagram to problems of tectonomagmatic classification and to establishing the nature of crustal contamination of basaltic lavas of the British Tertiary volcanic province: Earth and Planetary Science Letters, v. 50, p. 11–30.